Scientific Report S-28
May 31, 1974

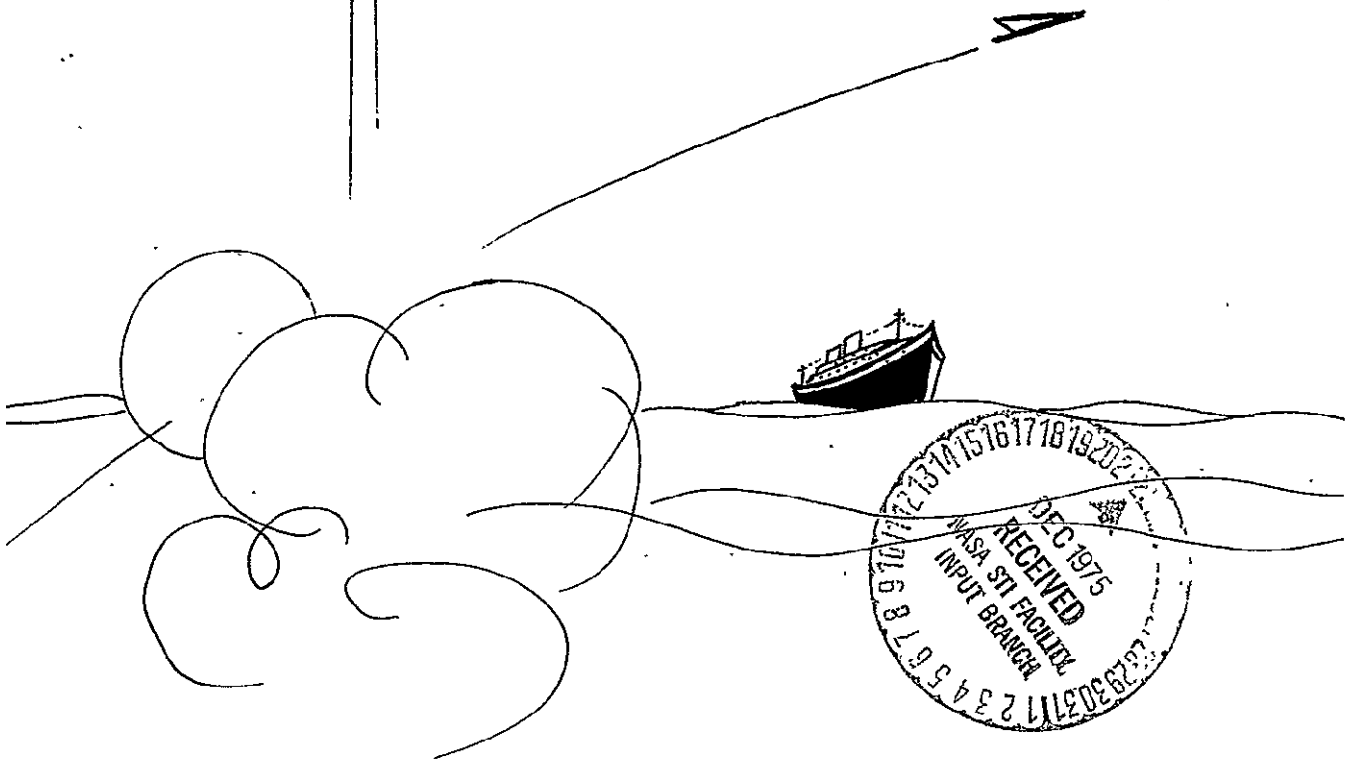

FEASIBILITY STUDY OF A DIGITAL REBALANCE LOOP FOR A DRY TUNED TDF GYRO

Prepared for George C. Marshall Space Flight Center, National Aeronautics and Space Administration under Contract NAS8-27296/DCN 1-1-40-10230

THE UNIVERSITY OF TENNESSEE
DEPARTMENT OF ELECTRICAL ENGINEERING

Scientific Report S-28
May 31, 1974

FEASIBILITY STUDY OF A DIGITAL REBALANCE LOOP FOR A DRY TUNED TDF GYRO

Prepared For
George C. Marshall Space Flight Center
National Aeronautics and Space Administration
Under Contract NAS8-27296/DCN 1-1-40-10230

D. E. Coffman

Department of Electrical Engineering
The University of Tennessee
Knoxville, Tennessee 37916

ACKNOWLEDGMENT

The author wishes to acknowledge the technical assistance of Dr. J.C. Hung, the preparation of the manuscript by Mrs. Nita Raulston and Mrs. Beverly Perry, all of U.T., and the encouragement of Mr. J.R. Parker of Marshall Space Flight Center, NASA.

ABSTRACT

A TDF rate integrating gyro in the strapdown mode is an attractive candidate for attitude sensing in a spacecraft navigation system, since it provides an additional axis of information for a relatively small increase in hardware complexity. A type of gyro which has not been fully exploited is of the dry, tuned, TDF design, in which the spring constant of the suspension system is effectively cancelled by the "dynamic anti-spring" of a swiveling, rotating, gimbal. The use of this unconventional gyro in a digital rebalance loop is investigated.

TABLE OF CONTENTS

LIST OF FIGURES

FIGURE PAGE

CHAPTER I

INTRODUCTION

The use of gyroscopes as attitude sensors in spacecraft applications is well known. Efforts to improve sensor performance while decreasing cost, weight, and power requirements are continuously being made. One such effort which has been successfully exploited is the strapdown concept,[1] in which the gimballed platform upon which the gyros reside is functionally replaced by an electronic rebalance loop for each gyro. This loop senses float motion away from a null position with respect to the case and applies the correct amount of current to the torquer coils to drive the float back to null, or rebalance it. Since the gyro floats' attitude with respect to the case is invariant, the case may be mounted to the spacecraft frame, eliminating the need of a separate platform. Thus the gimballed platform is said to be replaced by a computer, or analytical platform, and the quantity of sensor, and spacecraft, motion is found by measuring the torquing current. The advantage of the strapdown concept is that mechanical components are replaced with electronic components with an improvement in cost, weight, and reliability.

Although single-degree of freedom (SDF) floated gyros are presently used in strapdown systems, two-degree of freedom design would give another axis of information at a nominal increase in cost and weight. Conventional TDF floated gyros for platform use have not been adapted to strapdown applications because of difficulty in torquer design. The unconventional mechanical design described in this report utilizes a tuned suspension which eliminates the need for rotor flotation, high quality bearings, and elaborate gimbals. This design utilizes an inside-out construction in which the gyro rotor is external to its support and drive mechanisms, making torquer design easy to implement. In fact, this dry, tuned TDF gyro is ideally suited to strapdown applications since its limited angular range requires a rebalance loop.

In rebalance loops for strapdown applications, a digital torquing scheme commonly used is known as a pulse torque servo amplifier (PTSA). Accurately known current pulses are delivered to the torquer coil. The advantages of using a PTSA are twofold:

1. Because the current is either zero, or a positive or negative maximum, non-linearity of the torquer coil is eliminated as a source of scale factor error.

2. The current pulses may be counted to indicate the restoring torque necessary for rebalance, and consequently the sensor motion. This technique eliminates the need for additional analog to digital conversion, provided the pulse quantization is fine enough for the required data resolution.

Toward the goal of using a TDF dry tuned gyro as a strapdown instrument, a feasibility study for a PTSA loop is included in this report. For a better understanding of the control problem the transfer function of a tuned gyro is derived. As an example of a practical rebalance loop, the U.T. binary width modulated loop can be modified for use on a TDF dry tuned gyro.

CHAPTER II

DYNAMICS OF A DRY TUNED TDF GYRO

I. DESCRIPTION OF THE TUNED GYRO

In the early 1960's the need for a relatively inexpensive, light weight, rate-integrating gyro was recognized for use as an inertial sensor.[2,3,4,5] Conventional floated gyro technology had become sophisticated to the extent that additional improvements were very expensive. Undesirable effects, such as rotor mass unbalance caused by asymmetry of the windings on the spin motor, spring restoring torques caused by the motor power leads, and temperature effects caused by thermal gradients of the floatation fluid, could not be reduced easily and cheaply. Thus the stage was set for a radical departure from conventional gyro design philosophy.

This new philosophy produced a "tuned" gyro (Figure 2-1A) in which the rotor, coupled by a rotating, bearingless, suspension system to the drive shaft and motor, is "outside" its support mechanism, rather than inside, as in conventional design. The suspension system consists of a single ring, or gimbal, connected to the shaft and rotor by elastic restraints which have finite stiffness in torsion (twist) and infinite stiffness in flexure (bending). The axes of these restraints are orthogonal. It is the inertial reaction torque generated by the motion of the gimbal relative to the rotor and shaft effectively cancelling the elastic torque generated by twisting the restraints, which allows the rotor to be free, that is, torsionally decoupled from the shaft about its axes of freedom. This inertial reaction torque is sometimes called a dynamic antispring.

The tuned gyro is termed unconventional, or inside out, to distinguish it from the conventional gyro (Figure 2-1B), in which the rotor, and its spin motor, to which it is directly coupled, are inside the support mechanism. These gimbals do not spin with the rotor, as in the tuned case, rather they decouple the rotor from the case through

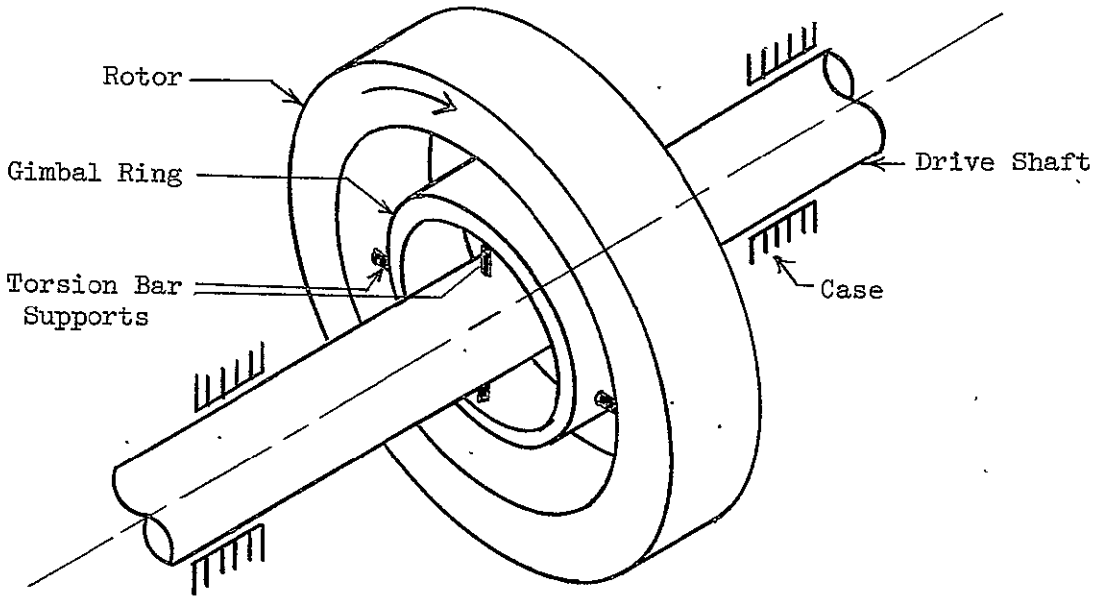

A. Tuned Gyro

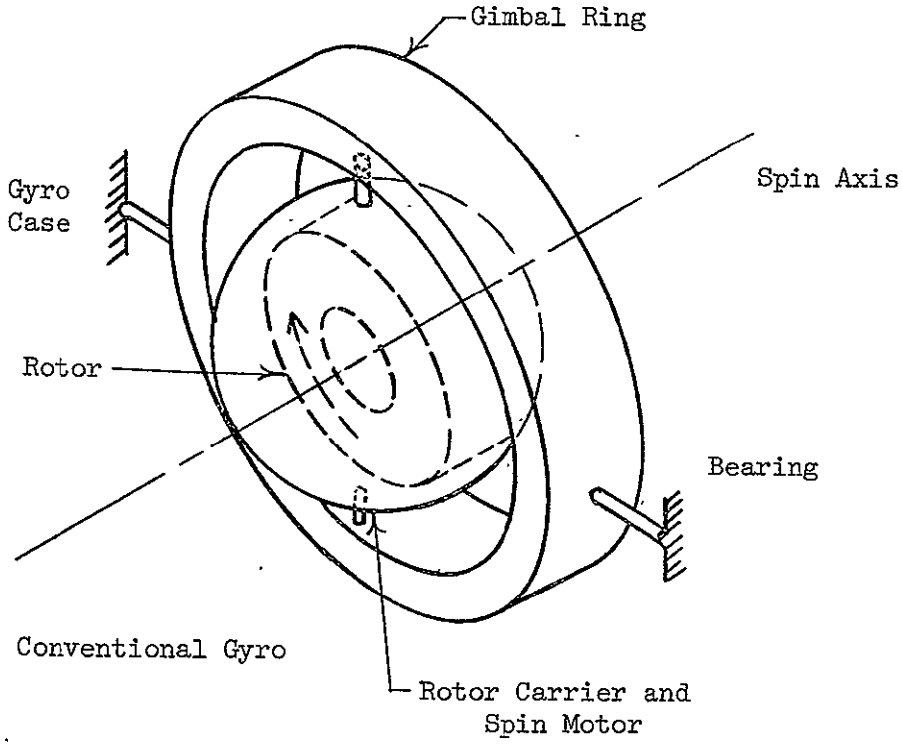

B. Conventional Gyro

Figure 2-1. Comparison of Conventional and Tuned Gyro

high quality bearings mounted on orthogonal axes. A gyro used in navigation and guidance systems must have a highly refined suspension for the rotor. One widely used means of "floating" the rotor consists of suspending a sealed housing containing the rotor and a spin motor in a high density fluid. The tuned gyro, which does not require flotation, is called "dry".

The principle difference between conventional and tuned gyros is the physical phenomena utilized. Conventional gyro design has exploited every means to provide the perfect bearing, while tuned gyros use the dynamics of the suspension system to give decoupling.

II. THE DYNAMIC ANTISPRING

The gimbal motion which generates the inertial reaction torque is simple harmonic with a frequency equal to twice the spin frequency. Figure 2-2 illustrates this motion, in which the gimbal plane experiences a complete period of its oscillation during one-half a rotor revolution because the axes of the restraints coincide after one-half revolution.

Analytically, the antispring may be observed in the equations of motion resulting from the gimbal action described in the preceeding paragraph. These equations[4] of motion are

$$\left.\begin{aligned}
&(A + A_g/2)\,\ddot{\theta}_X + D\dot{\theta}_X + [K - N^2(A_g - C_g/2)]\,\theta_X + \\
&N(C + A_g)\,\dot{\theta}_Y + T_D\theta_Y = -\frac{1}{2}[A_g\ddot{\theta}_X + 2A_gN\dot{\theta}_Y - \\
&(2A_g - C_g)\,N^2\theta_Y]\cos 2N - \frac{1}{2}[A_g\ddot{\theta}_Y - 2A_gN\dot{\theta}_X - \\
&(2A_g - C_g)\,N^2\theta_Y]\sin 2N + G_X \\
&\text{and}
\end{aligned}\right\} \quad (2\text{-}1)$$

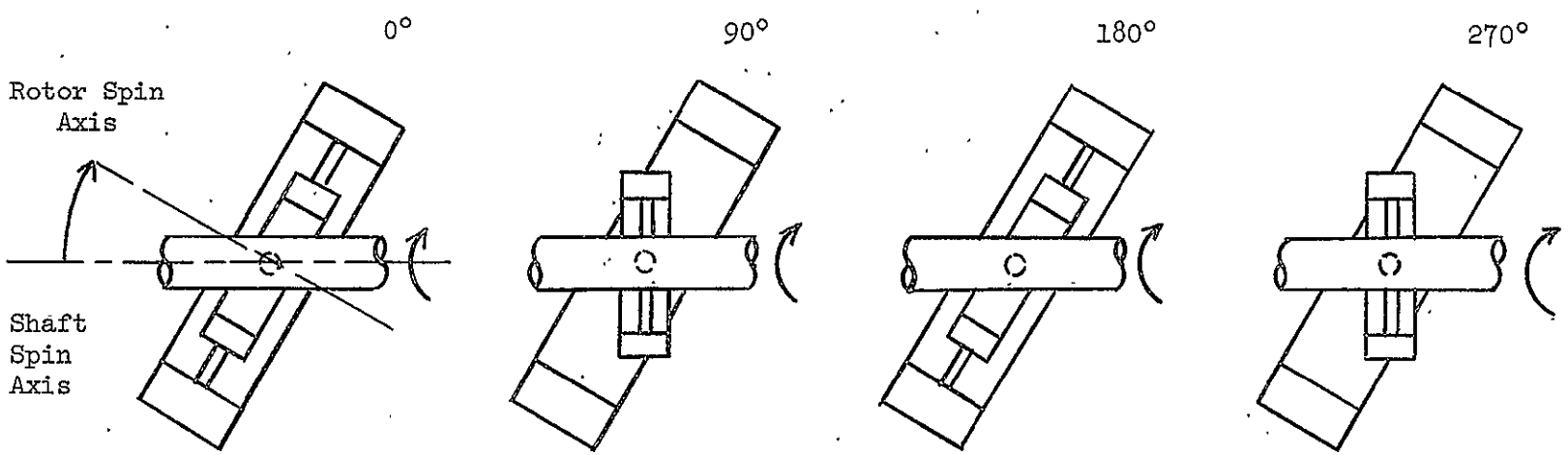

Figure 2-2. Simple Harmonic Motion of the Gimbal

$$(A + A_g/2)\ddot{\theta}_Y + D\dot{\theta}_Y + [K - N^2(A_g - C_g/2)]\theta_Y - N(C + A_g)\dot{\theta}_X - T_D\theta_X = \frac{1}{2}[A_g\ddot{\theta}_Y - 2A_gN\dot{\theta}_X - (2A_g - C_g)N^2\theta_Y]\cos 2N - \frac{1}{2}[A_g\ddot{\theta}_X + 2A_gN\dot{\theta}_Y - (2A_g - C_g)N^2\theta_X]\sin 2N + G_Y. \quad (2\text{-}1)$$

continued

θ_X and θ_Y are angular deflections of the rotor about the case-fixed X and Y axes, in response to G_X and G_Y, externally applied torques to rotor about these same axes. N is the spin frequency of the gyro, and all other terms are physical constants; C, A, C_g, and A_g spin and cross axis moments of inertia of the rotor and gimbal, respectively; D, viscous damping; K, spring constant; and T_D, the rotor-to-case drag coefficient. The dynamic antispring term, $-N^2(A_g - C_g/2)$, is always negative because A_g must be greater than $C_g/2$ (except for a gimbal of zero thickness, where $A_g = C_g/2$). If the spring constant equals the dynamic antispring, the torque-free operation is obtained provided the second harmonic terms in (2-1) can be neglected, and the gyro is said to be tuned. If these terms cannot be neglected, as in the case where G_X or G_Y contains 2N frequency components, then an unstable steady-state solution is obtained, because there is no positive spring constant term to cancel the antispring term in these second harmonic coefficients. This phenomenon is called the 2N sensitivity of the tuned gyro.

III. TRANSFER FUNCTION OF A SINGLE GIMBAL TUNED GYRO

A useful mode of operation of the gyro as a sensor is the strap-down mode, in which the gyro is strapped directly to the vehicle, rather than being mounted on a gimballed platform, and a rebalance torque applied to the rotor to maintain its attitude with respect to the vehicle fram. Attitude sensing is obtained by measuring the torque current necessary to rebalance the gyro. Accurate attitude information

depends on knowledge of the gyro transfer function. To give the reader a better understanding of the dynamics involved in a tuned gyro, a detailed derivation of its transfer function will be given.

In this section the coupled differential equations of motion in rotating coordinates will be derived for a single gimbal gyro. These differential equations will then be transformed into a transfer function relating case-fixed variables via a method using symmetrical components and a complex coordinate system.[6,7] The moment equations are derived in a shaft-fixed frame rotating at spin velocity because the dynamics of the rotating suspension system are easier to visualize in this frame. The method of symmetrical components provides a useful means to analyze systems with asymmetries, while the complex coordinate system is easy to use for the transformation between a rotating and stationary frame.

Moment Equations

Four coordinate systems (Figure 2-3) are needed for this derivation:

(X,Y,Z) ---- A case-fixed system, with its Z axis along the shaft spin-axis.

(x,y,z) ---- A shaft-fixed system, with z along the shaft spin-axis and x along the inner restraint.

(x_g,y_g,z_g) - A gimbal-fixed system, with x_g along the inner restraint axis and y_g the outer.

(x',y',z') - A rotor fixed system, with y' along the outer restraint axis and z' the rotor spin axis.

Figure 2-4 shows the detailed relation between case and shaft systems, in which the x and y axes rotate at N, the spin velocity, in the plane formed by the X and Y axes. The relation between the absolute angular velocity of the shaft, $\underline{\omega}$, resolved along the shaft set, and the absolute case velocity, $\underline{\dot{\phi}}$, resolved along the case set, is expressed with the aid of the Euler-angle transformation as

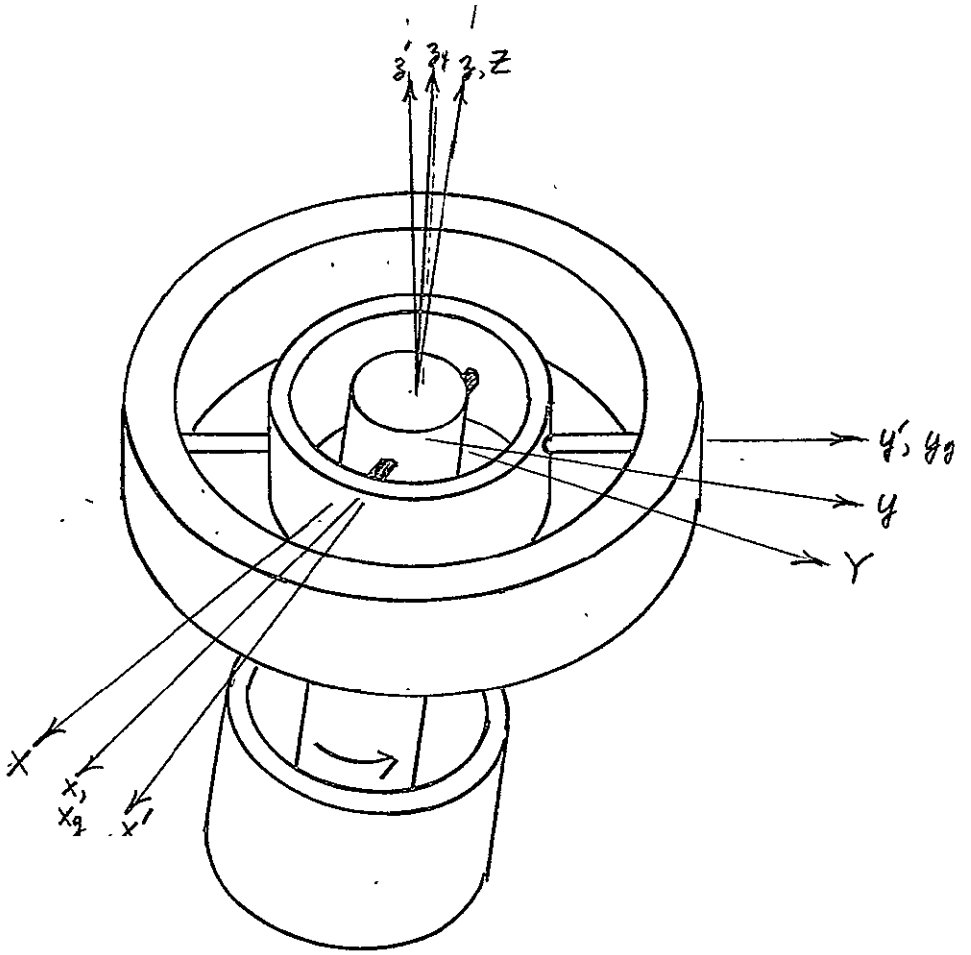

X, Y, Z - Imbedded in Case (non-rotating)

x, y, z - Imbedded in Shaft (rotating at N radians/sec)

x_g, y_g, z_g - Imbedded in Gimbal (rotates and moves with gimbal)

x´, y´, z´ - Imbedded in Rotor (rotates and moves with rotor)

Figure 2-3. Coordinate Frames Defined

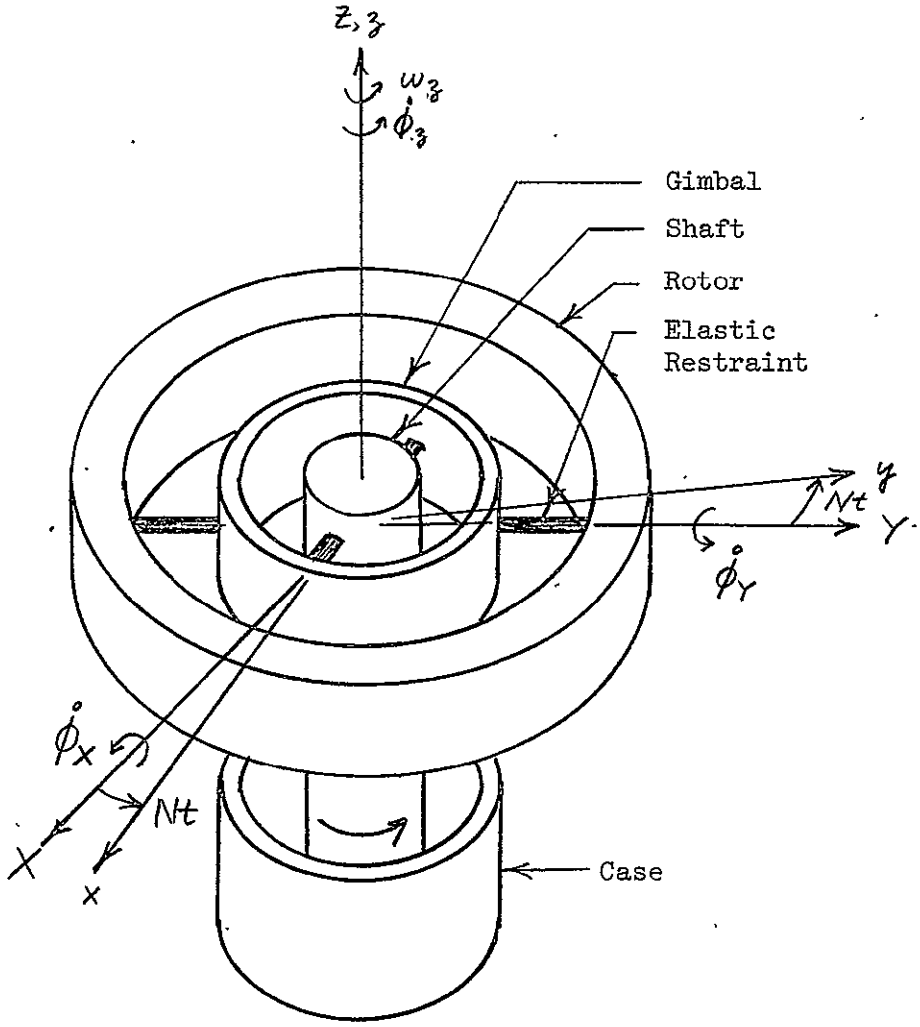

Figure 2-4. Relating Case and Shaft Coordinate Frames

$$\underline{\omega} = \begin{bmatrix} \omega_x \\ \omega_y \\ \omega_z \end{bmatrix} = \begin{bmatrix} \dot{\phi}_X \cos Nt + \dot{\phi}_Y \sin Nt \\ -\dot{\phi}_X \sin Nt + \dot{\phi}_Y \cos Nt \\ N + \dot{\phi}_Z \simeq N \end{bmatrix} , \tag{2-2}$$

where $\underline{\omega} = \begin{bmatrix} \omega_x \\ \omega_y \\ \omega_x \end{bmatrix}$ and $\dot{\underline{\phi}} = \begin{bmatrix} \dot{\phi}_X \\ \dot{\phi}_Y \\ \dot{\phi}_Z \end{bmatrix}$.

In Figure 2-5, the rotor is slightly tilted with respect to the shaft, such that angular displacements θ_X and $\theta_{y'}$ have been made about the x and y′ axes, respectively. The absolute rotor angular velocity, $\underline{\omega}'$, resolved along the rotor set, may be expressed as

absolute rotor velocity along rotor set	=	absolute shaft velocity along rotor set	+	rotor velocity with respect to shaft along rotor set

or

$$\underline{\omega}' = \underline{\omega}_{(r)} + \omega_{rs(r)} . \tag{2-3}$$

The term $\underline{\omega}_{(r)}$ may be expressed in terms of $\underline{\omega}$, as

$$\underline{\omega}_{(r)} = \begin{bmatrix} \cos\theta_{y'} & 0 & \sin\theta_{y'} \\ 0 & 1 & 0 \\ \sin\theta_{y'} & 0 & \cos\theta_{y'} \end{bmatrix} \begin{bmatrix} 1 & 0 & 0 \\ 0 & \cos\theta_x & \sin\theta_x \\ 0 & -\sin\theta_x & \cos\theta_x \end{bmatrix} \begin{bmatrix} \omega_x \\ \omega_y \\ \omega_z \end{bmatrix} . \tag{2-4}$$

In a tuned gyro, the angular deflections are small (in practice less than 5°), since this is a null type instrument, in which rebalance torques are used to make θ_x and θ_y approach zero. Therefore, the following small angle approximations are valid:

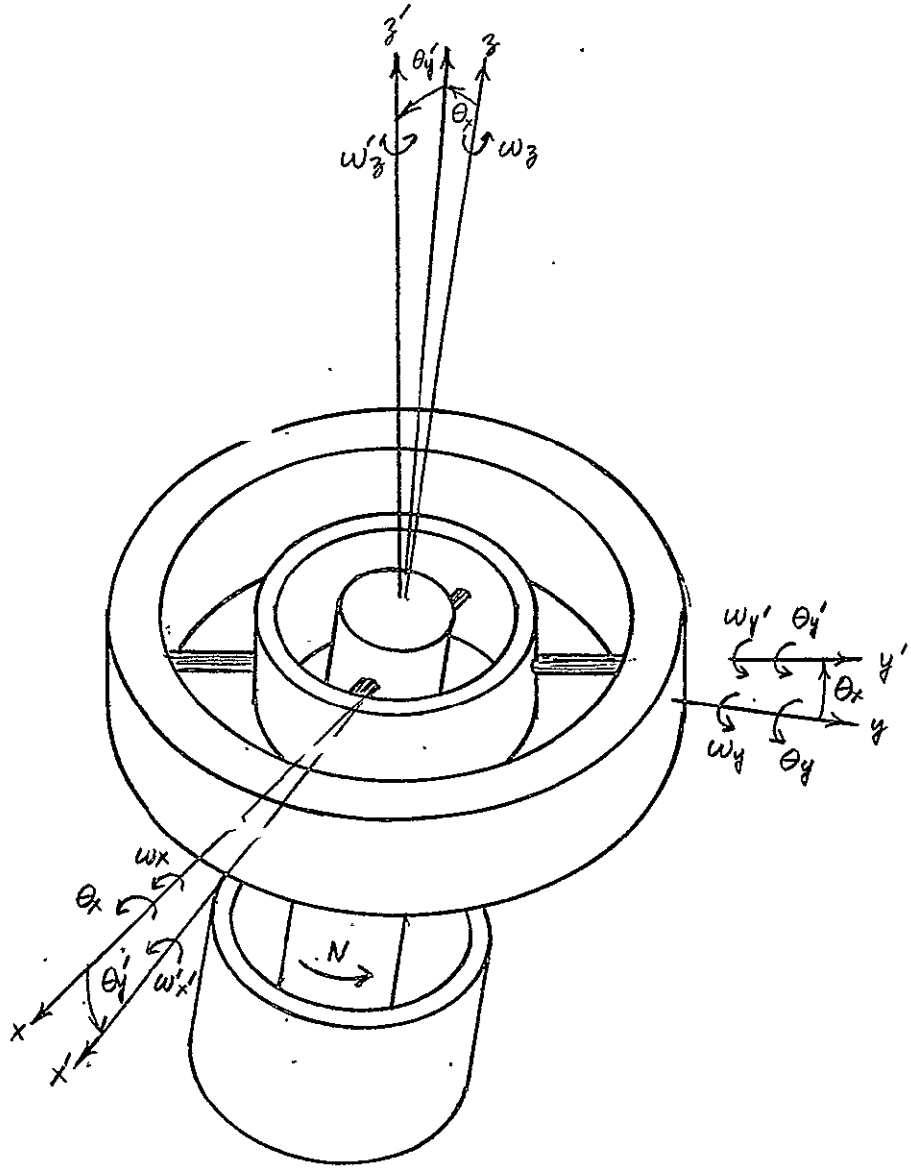

Figure 2-5. Relating the Rotor and Shaft Frames

$$
\begin{aligned}
&\theta_y' \approx \theta_y \\
&\cos\theta_x \approx 1,\ \cos\theta_y' \approx 1 \\
&\sin\theta_x \approx \theta_x,\ \sin\theta_y' \approx \sin\theta_y \approx \theta_y \\
&\theta_y'\theta_x \approx 0
\end{aligned}
\tag{2-5}
$$

Thus, (2-4) may be reduced to

$$
\underline{\omega}_{(r)} = \begin{bmatrix} 1 & 0 & -\theta_y \\ 0 & 1 & 0 \\ \theta_y & 0 & 1 \end{bmatrix} \begin{bmatrix} 1 & 0 & 0 \\ 0 & 1 & \theta_x \\ 0 & -\theta_x & 1 \end{bmatrix} \begin{bmatrix} \dot{\omega}_x \\ \omega_y \\ \omega_z \end{bmatrix} = \begin{bmatrix} 1 & 0 & -\theta_y \\ 0 & 1 & \theta_x \\ \theta_y & -\theta_x & 1 \end{bmatrix} \begin{bmatrix} \omega_x \\ \omega_y \\ \omega_z \end{bmatrix} . \tag{2-6}
$$

The second term on the right side of (2-3) allows time variations of θ_x and θ_y' and is

$$
\underline{\omega}_{rs(r)} = \begin{bmatrix} \cos\theta_y' \\ \cos 90 \\ \sin\theta_y' \end{bmatrix} \dot{\theta}_x + \begin{bmatrix} \cos 90 \\ \cos\theta_x \\ \sin\theta_x \end{bmatrix} \dot{\theta}_y = \begin{bmatrix} \dot{\theta}_x \\ \dot{\theta}_y \\ \theta_y\dot{\theta}_x + \theta_x\dot{\theta}_y \end{bmatrix} , \tag{2-7}
$$

using the small angle approximations. Adding (2-7) to (2-6), and observing that

$$
\omega_z \approx N >> \theta_y\dot{\theta}_x + \theta_x\dot{\theta}_y + \omega_x\theta_y - \omega_y\theta_x,
$$

(2-3) becomes

$$
\underline{\omega}' = \begin{bmatrix} \omega'_x \\ \omega'_y \\ \omega'_z \end{bmatrix} = \begin{bmatrix} \omega_x - N\theta_y + \dot{\theta}_x \\ \omega_y + N\theta_x + \dot{\theta}_y \\ N \end{bmatrix} . \tag{2-8}
$$

Figure 2-6 shows a top view of the gyro and a detailed relation between the shaft, gimbal, and rotor sets. Note that if the rotor is not tilted, θ_x and θ_y' equal zero, and these sets are coincident.

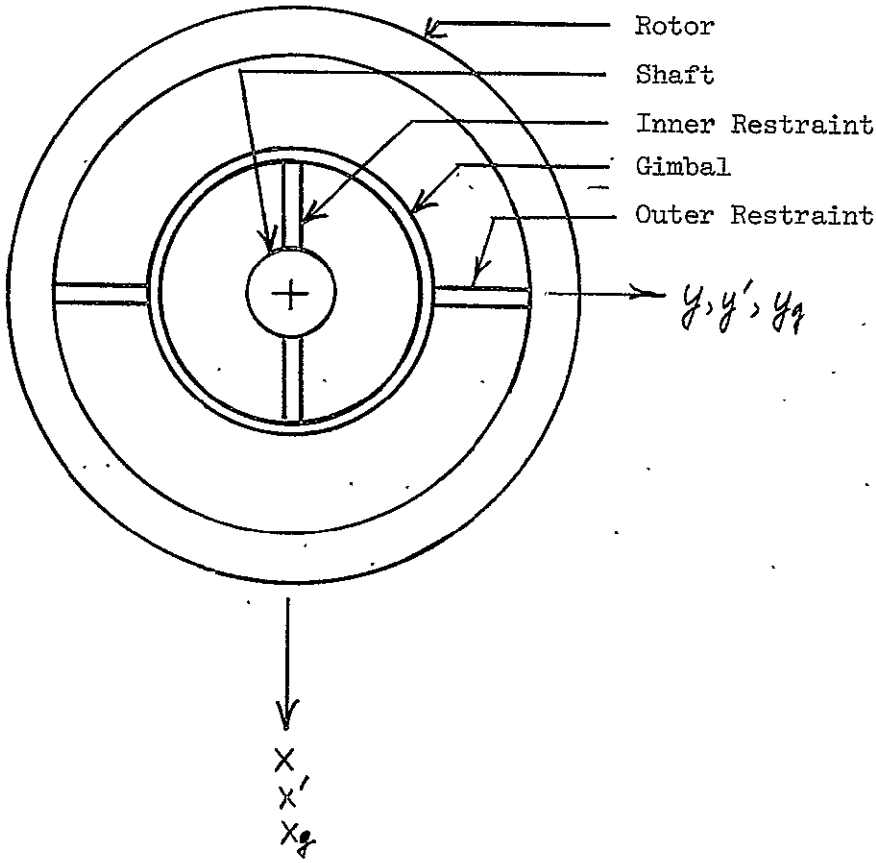

Figure 2-6. Illustrating Gimbal Set

The absolute angular rate of the gimbal, $\underline{\omega}_g''$, resolved along the gimbal set, is

Absolute Gimbal Velocity Along Gimbal Set	=	Absolute Shaft Velocity Along Shaft Set	+	Gimbal Velocity with respect to shaft along Gimbal Set

or

$$\underline{\omega}_g = \underline{\omega}_{(g)} + \underline{\omega}_{gs(g)}. \tag{2-9}$$

Using the same rationale as previously,

$$\underline{\omega}_{(g)} = \begin{bmatrix} 1 & 0 & -\theta_{yg} \\ 0 & 1 & \theta_{xg} \\ \theta_{yg} & -\theta_{xg} & 1 \end{bmatrix} \begin{bmatrix} \omega_x \\ \omega_y \\ \omega_z \end{bmatrix} \tag{2-10}$$

and

$$\underline{\omega}_{gs(g)} = \begin{bmatrix} \dot{\theta}_{xg} \\ \dot{\theta}_{yg} \\ \dot{\theta}_{zg} \end{bmatrix} \tag{2-11}$$

The inner elastic restraints cause the shaft and gimbal axes, x and x_g, to coincide, while the outer restraints cause the gimbal and rotor axes, y_g and y'', to coincide. Thus the angles

$$\theta_{xg} = \theta_x,$$
$$\theta_{yg} = 0,$$

and their derivatives,

$$\dot{\theta}_{xg} = \dot{\theta}_x,$$
$$\dot{\theta}_{yg} = 0$$

may be used with (2-10) and (2-11) to give

$$\underline{\omega}_g = \begin{bmatrix} \omega''_{xg} \\ \omega''_{yg} \\ \omega''_{zg} \end{bmatrix} = \begin{bmatrix} \omega_x + \dot{\theta}_x \\ \omega_y - N\theta_x \\ N \end{bmatrix}. \qquad (2\text{-}12)$$

Figure 2-7A shows a free body diagram of the gimbal used to derive its moment equations with respect to the gimbal coordinates. These moment equations, about the x_g and y_g axes, respectively, are

$$\left.\begin{aligned} T_{xg} - T_{xg'} &= A_g \dot{\omega}''_{xg} + (C_g - B_g)\, \omega''_{yg}\, \omega''_{zg} \\ \text{and} \\ T_{yg} - T_{yg'} &= B_g \dot{\omega}''_{yg} - (C_g - A_g)\, \omega''_{xg}\, \omega''_{zg}, \end{aligned}\right\} (2\text{-}13)$$

where the T_{xy} and T_{yg} are from the rotor via the outer restraints, and $T_{x'g}$ and $T_{y'g}$ from the shaft via the inner restraints, and A_g, B_g, and C_g represent moments of inertia about the x_g, y_g, and z_g axes, respectively. A_g and B_g are called cross-axis, while C_g is called a spin-axis moment of inertia. The twisting moments yield the following torque equations,

$$\left.\begin{aligned} T_{x'g} &= K_x \theta_{x'} + D_x \dot{\theta}_{x'} \\ T_{yg} &= K_y \theta_{y'} + D_y \dot{\theta}_{y'} \end{aligned}\right\} (2\text{-}14)$$

where $\theta_{x'} = \theta_x$, $\theta_{y'} \approx \theta_y$, and K_x and K_y are spring constants, and D_x and D_y viscous damping. Substituting (2-14) into (2-13) gives

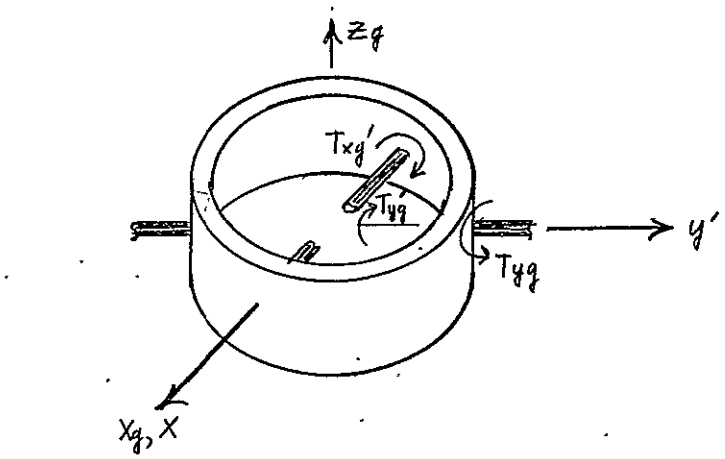

A. Gimbal

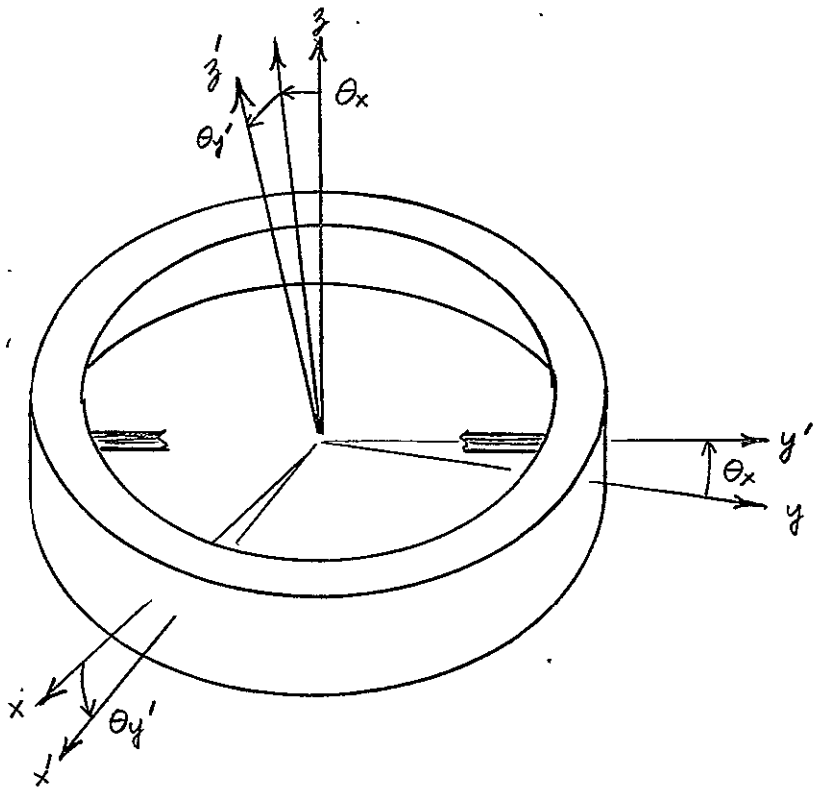

B. Rotor

Figure 2-7. Free Body Diagrams of the Gimbal and Rotor

$$\left.\begin{aligned} T_{xg} &= A_y \dot{\omega}''_{xg} + (C_g - B_g)\, \omega''_{yg}\, \omega''_{zg} + K_x \theta_x + D_x \dot{\theta}_x \\ -T_{y'g} &= B_y \dot{\omega}''_{yg} - (C_g - A_g)\, \omega''_{xy}\, \omega''_{zg} - K_y \theta_y - D_y \dot{\theta}_y \end{aligned}\right\} \quad (2\text{-}15)$$

From Figure 2-7B, the moment equations of the rotor about the x' and y' axes are

$$\left.\begin{aligned} M_{x'} &= A\dot{\omega}_{x'} + (C - B)\, \omega_{y'}\, \omega_{z'} + T_{x'} + T_D \sin \theta_{y'} \\ \text{and} \\ M_{y'} &= B\dot{\omega}_{y'} - (C - A)\, \omega_{x'}\, \omega_{z'} + T_{y'} - T_D \sin \theta_{x'} \end{aligned}\right\} \quad (2\text{-}16)$$

where $M_{x'}$ and $M_{y'}$ are externally applied moments, A, B, and C, rotor moments of inertia, $T_{x'}$ and $T_{y'}$ torques applied through the suspension, and T_D the rotor drag torque. For small θ_x and $\theta_{y'}$,

$$M_{x'} \simeq M_x \text{ and } M_{y'} \simeq M_y,$$

$$T_{x'} \simeq T_{xg} \text{ and } T_{y'} \simeq T_{yg},$$

and (2-16) becomes

$$\left.\begin{aligned} M_x &= A\dot{\omega}_{x'} + (C - B)\, \omega_{y'}\omega_{z'} + A_g\dot{\omega}''_{xg} + (C_g - B_g)\, \omega''_{yg}\omega''_{zg} + \\ &\quad K_x\theta_x + D_x\dot{\theta}_x + T_D\theta_y \\ M_y &= B\dot{\omega}_{y'} - (C - A)\, \omega_{x'}\omega_{z'} + K_y\theta_y + D_y\dot{\theta}_y - T_D\theta_x, \end{aligned}\right\} \quad (2\text{-}17)$$

where the first of (2-15) has been substituted for T_{xg}, the second of (2-14) for T_{yg}, and the small angle approximation used for sin θ_x and sin $\theta_{y'}$. Substituting (2-8) and (2-12) into (2-17) to get all angular velocities in terms of shaft rates gives

$$
\left.
\begin{aligned}
M_x &= A(\dot{\omega}_x + \ddot{\theta}_x - N\dot{\theta}_y) + (C - B)\,(\omega_y + \dot{\theta}_y + N\theta_x)\,N + \\
&\quad A_g(\dot{\omega}_x + \ddot{\theta}_x) + (C_g - B_g)\,(\omega_y + N\theta_x)\,N + K_x\theta_x \\
&\quad + D_x\dot{\theta}_x + T_D\theta_y, \\
M_y &= B(\dot{\omega}_y + \ddot{\theta}_y + N\dot{\theta}_x) - (C - A)\,(\omega_x + \dot{\theta}_x - N\theta_y)\,N + \\
&\quad K_y\theta_y + D_y\dot{\theta}_y - T_D\theta_x.
\end{aligned}
\right\} \quad (2\text{-}18)
$$

collecting terms with angles, velocities, and their derivatives as common factors, gives the coupled differential equations of motion of the rotor in shaft fixed coordinates:

$$
\left.
\begin{aligned}
&\ddot{\theta}_x(A + A_g) + \dot{\theta}_x D_x + \theta_x[K_x + N^2(C - B + C_g - B_g)] + \\
&\dot{\theta}_y N(C - B - A) + \theta_y T_D + \dot{\theta}_x(A + A_g) + \theta_y N(C - B + C_g - B_y) \\
&= M_x \\
&\ddot{\theta}_y(B) + \dot{\theta}_y D_y + \theta_y[K_y + N^2(C - A)] + \\
&\dot{\theta}_x N(C - B - A) - \theta_x T_D + \dot{\omega}_y B - \omega_x N(C - A) \\
&= M_y .
\end{aligned}
\right\} \quad (2\text{-}19)
$$

Transformation Using the Complex Method

To transform the coupled differential equations of (2-19) to a transfer function relating variables in a case-fixed frame, a complex plane technique will be used. First, define the following symmetrical components:

$$
\left.
\begin{aligned}
I &= (A + B + A_g)/2 \\
I' &= (A - B + A_g)/2
\end{aligned}
\right.
$$

$$
\begin{aligned}
D &= (D_x + D_y)/2 \\
D' &= (D_x - D_y)/2 \\
K &= (K_x + K_y)/2 \\
K' &= (K_x - K_y)/2 \\
J &= (2C - B - A + C_g - B_g)/2 \\
J' &= (A - B + C_g - B_g)/2 \\
L &= C - B - A \\
L' &= 0 \\
P &= (A + B + A_g)/2 \\
P' &= (A - B + A_g)/2 \\
R &= (2C - B - A + C_g - B_g)/2 \\
R' &= (A - B + C_g - B_g)/2
\end{aligned}
\qquad (2\text{-}20)
$$

Substituting (2-20) into (2-19),

$$
\begin{aligned}
M_x = {} & \ddot{\theta}_x(I + I') + \dot{\theta}_x(D + D') + \theta_x[K + K' + N^2(J + J')] + \\
& \dot{\theta}_y N(L + L')\theta_y T_D + \dot{\theta}_x(P + P') + \theta_y N(R + R') \\
M_y = {} & \ddot{\theta}_y(I - I') + \dot{\theta}_y(D - D') + \theta_y[K - K' + N^2(J - J')] \\
& \dot{\theta}_x N(L - L') - \theta_x T_D + \dot{\omega}_y(P - P') - \omega_x N(R - R').
\end{aligned}
\qquad (2\text{-}21)
$$

Next the equations of (2-21) are combined into a single equation by multiplying the second by $j = \sqrt{-1}$ and adding it to the first, using the following complex relations:

$$\left.\begin{aligned}
\theta_{xy} &= \theta_x + j\theta_y, \\
\omega_{xy} &= \omega_x + j\omega_y, \\
M_{xy} &= M_x + jM_y,
\end{aligned}\right\} \quad (2\text{-}22)$$

their conjugates,

$$\left.\begin{aligned}
\overline{\theta}_{xy} &= \theta_x - j\theta_y \\
\overline{\omega}_{xy} &= \omega_x - j\omega_y \\
\overline{M}_{xy} &= M_x - jM_y
\end{aligned}\right\} \quad (2\text{-}22)$$

and derivatives, and conjugate derivatives,

$$\left.\begin{aligned}
\dot{\theta}_{xy} &= \dot{\theta}_x + j\dot{\theta}_y, \\
\ddot{\theta}_{xy} &= \ddot{\theta}_x - j\ddot{\theta}_y, \\
\dot{\omega}_{xy} &= \dot{\omega}_x + j\dot{\omega}_y, \\
\dot{\overline{\omega}}_{xy} &= \dot{\omega}_x - j\dot{\omega}_y, \\
\dot{\overline{\theta}}_{xy} &= \dot{\theta}_x - j\dot{\theta}_y, \\
\ddot{\overline{\theta}}_{xy} &= \ddot{\theta}_x - j\ddot{\theta}_y.
\end{aligned}\right\} \quad (2\text{-}22)$$

$$\left.\begin{aligned}
M_{xy} = {} & I\ddot{\theta}_{xy} + I'\dot{\ddot{\theta}}_{xy} + (D - jNL)\,\dot{\theta}_{xy} + (D' + jNL')\,\dot{\overline{\theta}}_{xy} \\
& (K - N^2J - jT_D)\,\theta_{xy} + (K' - N^2J')\,\overline{\theta}_{xy} + P\dot{\omega}_{xy} + \\
& P'\dot{\overline{\omega}}_{xy} - jNR\omega_{xy} + jNR'\overline{\omega}_{xy}.
\end{aligned}\right\} \quad (2\text{-}23)$$

The Euler angle transformation from a shaft-fixed (rotating) frame to a case-fixed (non-rotating) frame for angles, rates, and their derivatives, are

$$\left.\begin{aligned}
\theta_{xy} &= \Theta_{XY}\varepsilon^{-jNt} \\
\dot{\theta}_{xy} &= (\dot{\Theta}_{XY} - jN\Theta_{XY})\varepsilon^{-jNt} \\
\ddot{\theta}_{xy} &= (\ddot{\Theta}_{XY} - j2N\dot{\Theta}_{XY} - N^2\Theta_{XY})\varepsilon^{-jNt}
\end{aligned}\right\} \quad (2\text{-}24)$$

$$\left.\begin{aligned}\omega_{xy} &= \dot{\phi}_{XY}\varepsilon^{-jNt} \\ \dot{\omega}_{xy} &= (\ddot{\phi}_{XY} - jN\dot{\phi}_{XY})\varepsilon^{-jNt},\end{aligned}\right]$$

while conjugation of the above relations simply conjugates each term of each relation, which changes the sign of the imaginary component. The externally applied moment minus the rotor damping is

$$M_{xy} = M_{XY}\varepsilon^{-jNt} - D_R\dot{\theta}_{XY}\varepsilon^{-jNt}. \tag{2-25}$$

Using the relations of (2-24) and (2-25) in (2-23) gives

$$\left.\begin{aligned}&\{I[\ddot{\theta}_{XY} - j2N\dot{\theta}_{XY} - N^2\theta_{XY}] + (D - jNL)(\dot{\theta}_{XY} - jN\theta_{XY}) \\ &+ (K + N^2J - jT_D)\theta_{XY} + D_R\dot{\theta}_{XY}\}\varepsilon^{-jNt} + \\ &\{I'[\ddot{\bar{\theta}}_{XY} + j2N\dot{\bar{\theta}}_{XY} - N^2\bar{\theta}_{XY}] + (D' + jNL')(\dot{\bar{\theta}}_{XY} + jN\bar{\theta}_{XY}) \\ &+ (K' + N^2J')\bar{\theta}_{XY}\}\varepsilon^{+jNt} = \\ &\{M_{XY} - P(\ddot{\phi}_{XY} - jN\dot{\phi}_{XY}) - jNR\dot{\phi}_{XY}\}\varepsilon^{-jNt} + \\ &\{-P'(\ddot{\bar{\phi}}_{XY} + jN\dot{\bar{\phi}}_{XY}) - jNR'\dot{\bar{\phi}}_{XY}\}\varepsilon^{+jNt}\end{aligned}\right] \tag{2-26}$$

which is the complex form of the rotor moment equation in case-fixed coordinates. The following Laplace transformations are useful:

$$\left.\begin{aligned}&L[f(t)] = F(s) \\ &L[f(t)e^{+j2Nt}] = F(s - j2N) \\ &L[\dot{f}(t)] = sF(s) \\ &L[\ddot{f}(t)] = s^2F(s) \\ &L[\dot{f}(t)\varepsilon^{j2Nt}] = (s - j2N)\,F(s - j2N) \\ &L[\ddot{f}(t)\varepsilon^{j2Nt}] = (s^2 - j4Ns - 4N^2)\,F(s - j2N)\end{aligned}\right\} \tag{2-27}$$

where initial conditions are assumed zero. Equation (2-26) is multiplied through by ε^{jNt} and Laplace transformed using (2-27), giving

$$\{I(s^2 - j2Ns - N^2) + (D - jNL)(s - jN) - jT_D + K + N^2J + D_Rs\}\,\theta_{XY}(s) + \{I'(s^2 - j2Ns - N^2) + (D' + jNL')(s - jN) + K' + N^2J'\}\,\bar{\theta}_{XY}(s - j2N) = M_{XY}(s) - \{P(s - jN) - jNR\}\,\dot{\phi}_{XY}(s) - \{P'(s - jN) + jNR'\}\,\dot{\bar{\phi}}_{XY}(s - j2N). \tag{2-28}$$

The coefficients of $\theta_{XY}s$, $\bar{\theta}_{XY}(s - j2N)$, $-\dot{\bar{\phi}}_{XY}(s)$, and $-\dot{\bar{\phi}}_{XY}(s - j2N)$ are defined as

$$\begin{aligned} Z_1(s) &= I(s^2 - j2Ns - N^2) + (D - jNL)(s - jN) + K + N^2J - jT_D + D_Rs \\ Z_2(s) &= I'(s^2 - j2Ns - N^2) + (D' + jNL')(s - jN) + K' + N^2J \\ Z_3(s) &= +\{P(s - jN) - jNR\} \\ Z_4(s) &= \{P'(s - jN) + jNR'\} \end{aligned} \tag{2-29}$$

Substituting (2-29) into (2-28) yields

$$Z_1(s)\theta_{XY}(s) + Z_2(s)\,\bar{\theta}_{XY}(s - j2N) = M_{XY}(s) - Z_3(s)\,\dot{\phi}_{XY}(s) - Z_4(s)\,\dot{\bar{\phi}}_{XY}(s - j2N). \tag{2-30}$$

Equation (2-30) is a statement in the complex frequency domain relating complex rotor angle $\theta_{XY}(s)$, and its conjugate at twice spin frequency, $\bar{\theta}_{XY}(s - j2N)$, to the complex case input rate, $\dot{\phi}_{XY}(s)$, and its 2N conjugate $\dot{\bar{\phi}}_{XY}(s - j2N)$, and externally applied complex moments, $M_{XY}(s)$. This equation may be solved for either the direct or 2N frequency component by the following means[6]:

1. Conjugate (2-30), using a dummy variable for s.
2. Substitute s - j2N for the dummy variable.
3. The new equation, which is

$$\bar{Z}_1(s - j2N)\,\bar{\theta}_{XY}(s - j2N) + \bar{Z}_2(s - j2N)\,\theta_{XY} = \bar{M}_{XY}(s - j2N) - \bar{Z}_3(s - j2N)\,\dot{\bar{\phi}}_{XY}(s - j2N) - \bar{Z}_4(s - j2N)\,\dot{\phi}_{XY}(s) \tag{2-31}$$

may be solved simultaneously with (2-30) to give either $\Theta_{XY}(s)$ or $\overline{\Theta}_{XY}(s - j2N)$. This solution , in matrix form, is

$$\begin{bmatrix} \Theta_{XY}(s) \\ \overline{\Theta}_{XY}(s - j2N) \end{bmatrix} = \begin{bmatrix} Z_1(s) & Z_2(s) \\ \overline{Z}_2(s - j2N) & \overline{Z}_1(s - j2N) \end{bmatrix}^{-1} \cdot \begin{bmatrix} M_{XY}(s) \\ \overline{M}_{XY}(s - j2N) \end{bmatrix} - \tag{2-32}$$

$$\begin{bmatrix} Z_1(s) & Z_2(s) \\ \overline{Z}_2(s - j2N) & \overline{Z}_1(s - j2N) \end{bmatrix}^{-1} \cdot \begin{bmatrix} Z_3(s) & Z_4(s) \\ \overline{Z}_4(s - j2N) & \overline{Z}_3(s - j2N) \end{bmatrix} \cdot \begin{bmatrix} \dot{\phi}_{XY}(s) \\ \dot{\overline{\phi}}_{XY}(s - j2N) \end{bmatrix}$$

Justification for the preceeding operation is given in Appendix A.

Solution of (2-32) is simplified using the following approximations:

1. Rotor to case drag, and damping coefficients are negligably small, therefore

$$T_D = D = D' = D_R = 0.$$

2. By symmetry,

$$A = B,$$

$$A_g = B_g,$$

and $$K_x = K_y$$

therefore, (2-20) becomes

$$I = A + A_g/2$$

$$I' = A_g/2$$

$$K' = 0$$

$$
\left.
\begin{aligned}
J &= C - A + 1/2\ C_g - 1/2\ A_g \\
J' &= C_g/2 - A_g/2 \\
L &= C - 2A \\
L' &= 0 \\
P &= 2A + A_g \\
P' &= A_g \\
R &= C - A + C_g/2 - A_g/2 \\
R' &= C_g/2 - A_g/2
\end{aligned}
\right\} \quad (2\text{-}33)
$$

and (2-29) may be simplified to

$$
\left.
\begin{aligned}
Z_1(s) &= s^2(A + A_g/2) - jNs(C + A_g) + N^2(A_g - C_g/2) \\
Z_2(s) &= s^2 A_g/2 - jNsA_g - N^2(A_g - C_g/2) \\
Z_3(s) &= s(A + A_g/2) - jN(C + C_g/2) \\
Z_4(s) &= sA_g/2 - jN(A_g - C_g/2).
\end{aligned}
\right\} \quad (2\text{-}34)
$$

conjugation and substitution of $s - j2N$ in (2-34) yields

$$
\left.
\begin{aligned}
\overline{Z}_1(s - j2N) &= s^2(A + A_g/2) - jNs(4A - C + A_g) + \\
&K - N^2(4A - 2C + A_g - C_g/2) \\
\overline{Z}_2(s - j2N) &= s^2 A_g/2 - jNsAg - N^2(A_g - C_g/2) \\
\overline{Z}_3(s - j2N) &= s(A + A_g/2) - j\,N\,(2A - C + A_g - C_g/2) \\
\overline{Z}_4(s - j2N) &= sA_g/2 - jNC_g/2.
\end{aligned}
\right\} \quad (2\text{-}35)
$$

Solution of (2-32) for $\Theta_{XY}(s)$ gives

$$
\left.
\begin{aligned}
\Theta_{XY}(s) = {} & \overline{Z}_1(s - j2N)\, M_{XY}(s) - Z_2(s)\, \overline{M}_{XY}(s - j2N) \\
& - [\overline{Z}_1(s - j2N)\, Z_3(s) - Z_2(s)\, \overline{Z}_4(s - j2N)]\, \dot{\phi}_{XY}(s) \\
& - [\overline{Z}_1(s - j2N)\, Z_4(s) - Z_2(s)\, \overline{Z}_3(s - j2N)]\, \dot{\overline{\phi}}_{XY}(s - j2N) \\
& [Z_1(s)\, \overline{Z}_1(s - j2N) - Z_2(s)\, Z_2(s - j2N)],
\end{aligned}
\right\} \quad (2\text{-}36)
$$

which is the complex form of the output angle, in case-fixed coordinates, as a function of input rates and moments.

Transfer Function

Reduction of (2-36) to a useful transfer function form, requires the following assumptions:

1. The rotor is thin, that is, $C = 2A$, which allows simplification of the terms $\bar{Z}_1(s - j2N)$ and $\bar{Z}_3(s - j2N)$.

2. Gimbal inertias are negligably small in comparison with rotor inertias, which allows the following simplifications:

   A. The product $Z_2(s) \cdot \bar{Z}_2(s - j2N)$ in the denominator may be neglected.

   B. The effect of $\bar{M}_{XY}(s - j2N)$ may be neglected because $Z_2(s)$ is small.

   C. The product $Z_2(s) \cdot \bar{Z}_4(s - j2N)$ in the coefficient of $\phi_{XY}(s)$ may be neglected.

   D. Because of A., the coefficient of $\dot{\bar{\phi}}(s - j2N)$ may be reduced to

$$-\frac{Z_4(s)}{Z_1(s)} \mp \frac{Z_2(s)}{Z_1(s) \cdot (s - j2N)} ,$$

   which, since it contains only gimbal terms in the numerator, may be neglected.

Use of the preceeding assumptions and the condition of tuning,

$$K = N^2(A_g - C_g/2), \tag{2-37}$$

to eliminate the constant terms in $Z_1(s)$ and $\bar{Z}_1(s - j2N)$, reduces (2-36) to

$$\Theta_{XY}(s) = \frac{M_{XY}(s)}{As(s - j2N)} - \frac{\dot{\phi}_{XY}(s)}{s} . \tag{2-38}$$

Equation (2-38) may be transformed using (2-22) into

$$\left.\begin{aligned} \theta_X(s) &= \frac{M_X(s)/A}{s^2 + 4N^2} - \frac{(2N/A) \cdot M_Y(s)}{s(s^2 + 4N^2)} - \frac{\dot{\phi}_X(s)}{s} \\ \theta_Y(s) &= \frac{M_X(s) \cdot 2N/A}{s(s^2 + 4N^2)} + \frac{M_Y(s)/A}{s^2 + 4N^2} - \frac{\dot{\phi}_Y(s)}{s} \end{aligned}\right\} \quad (2\text{-}39)$$

which is the transfer function[7] of a two-degree-of-freedom rate integrating gyro.

Transfer Function Including 2N Rate and Moment Inputs

Some of the preceeding approximations used to simplify the transfer function of a tuned gyro are inappropriate. In a gyro used in the strapdown mode,[8] Figure 2-8, the rebalance torque is applied with a magnetic force, and proper design must provide an efficient magnetic circuit for the torquer flux. Consequently, the rotor is not thin, that is, $2A \neq C$. For the rotor of Figure 2-8, 2A is about 10% greater than C, and the quantity $2A - C$ cannot be neglected in $\overline{Z}_1(s - j2N)$ and $\overline{Z}_3(s - j2N)$, since it is large compared with $A_g - C_g/2$.

Although higher ordered terms of $Z_2(s) \cdot \overline{Z}_2(s - j2N)$ may be neglected in comparison with those of $Z_1(s) \cdot \overline{Z}_1(s - j2N)$, its constant term must be considered. The condition of tuning, which forces the constant term of the characteristic equation $(Z_1(s)\,\overline{Z}_1(s - j2N) - Z_2(s) \cdot \overline{Z}_2(s - j2N))$ to zero is

$$K = N^2\{(A_g - C_g/2 + 2A - C) \pm [(A_g - C_g/2)^2 + (2A - C)^2]^{1/2}\}. \quad (2\text{-}40)$$

Other terms of the characteristic equation are

$$A^2s^4 - jN4A^2s^3 - N^2 4A^2s^2 \pm j4N^3A\,[(A_g - C_g/2)^2 + (2A - C)^2]^{1/2}s, \quad (2\text{-}41)$$

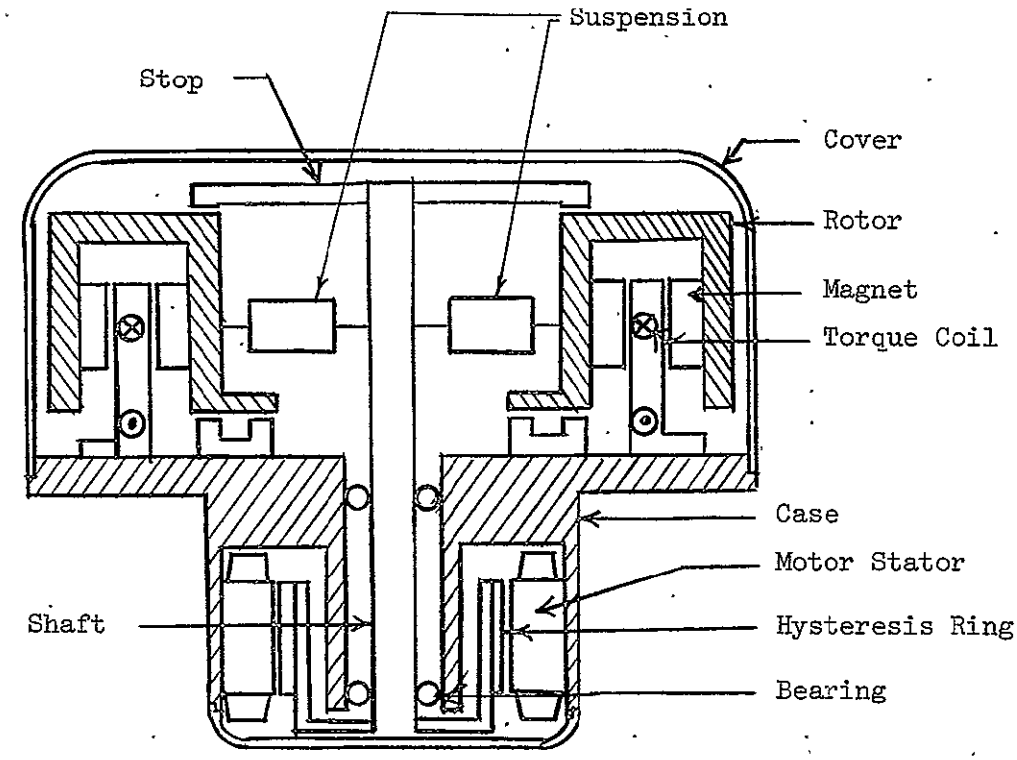

Figure 2-8. Cross Section of Teledyne Gyro

in which the constant term is negligably small, leaving

$$A^2s^2(s - j2N)^2 \tag{2-42}$$

as the characteristic equation. The numerator of the transfer function is

$$\begin{aligned} &-A^2s[s^2 - j4Ns - 4N^2]\,\dot{\phi}_{XY}(s) + As(s - j2N)\,M_{XY}(s) \\ &+ jNA(A_g - C_g/2)\,s(s - jN)\,\dot{\bar{\phi}}_{XY}(s - j2N) \\ &+(A_g/2)\,s(s - j2N)\,\bar{M}_{XY}(s - j2N), \end{aligned} \tag{2-43}$$

where the constant terms are considered negligably small, because they contain inertial differences due to finite thickness, i.e., $A_g - C_g/2$ and $A - C/2$, or in the case of the $\dot{\bar{\phi}}_{XY}(s - j2N)$ term, the product of these differences. The transfer function may be resolved into its X and Y components, giving

$$\begin{aligned} \Theta_X(s) = &-\frac{\dot{\phi}_X(s)}{s} + \frac{sM_X(s) - 2N \cdot M_Y(s)}{As(s^2 + 4N^2)} - \\ &\frac{A_g/2}{A} \cdot \frac{sM_X(s - j2N) + 2N \cdot M_Y(s - j2N)}{As(s^2 + 4N^2)} - \\ &N(A_g - C_g/2) \cdot \frac{(3N\,s^2 + 4N^3)\,\dot{\phi}_X(s - j2N) - s^3\,\dot{\phi}_Y(s - j2N)}{As(s^2 + 4N^2)^2}, \end{aligned}$$

and (2-44)

$$\theta_Y(s) = -\frac{\dot{\phi}_Y(s)}{s} + \frac{2N \cdot M_X(s) + sM_Y(s)}{As(s^2 + 4N^2)} +$$

$$\frac{A_g/2}{A} \cdot \frac{2N \cdot M_X(s - j2N) - s \cdot M_Y(s - j2N)}{As(s^2 + 4N^2)} -$$

$$N(A_g - C_g/2) \cdot \frac{-s^3 \ddot{\phi}_X(s - j2N) - (3Ns^2 + 4N^3) \dot{\phi}_Y(s - j2N)}{As(s^2 + 4N^2)^2}$$

Equations (2-44) contain all the terms of (2-39) plus additional terms to account for external moments and input rates at twice the spin frequency. Of particular importance are the terms related to 2N rate inputs. An impulse rate input about either axis at 2N (a sinusoidal angular displacement of constant amplitude and frequency of 2N) gives outputs about both axes which have a non-zero average value. This phenomenon is known as 2N rectification, and generates a drift error in the gyro used as a sensor. The terms related to 2N moment inputs are not particularly important, because moment inputs are controlled by currents in the torques, and the designer can eliminate currents at this frequency. A block diagram of (2-40) is shown in Figure 2-9.

IV. TRANSFER FUNCTION OF A TWO GIMBAL TUNED GYRO

For the single gimbal gyro with a thick rotor (2A > C), the tuning condition (2-40) contains rotor inertias, indicating that rotor dynamics enters the design of a single gimbal tuned gyro. The addition of a second gimbal and pair of restraints (Figure 2-10) allows the designer to eliminate rotor terms from the tuning equation and 2N rectification from the output.

Moment Equations

The second gimbal adds another coordinate system to the four considered for the single gimbal case,

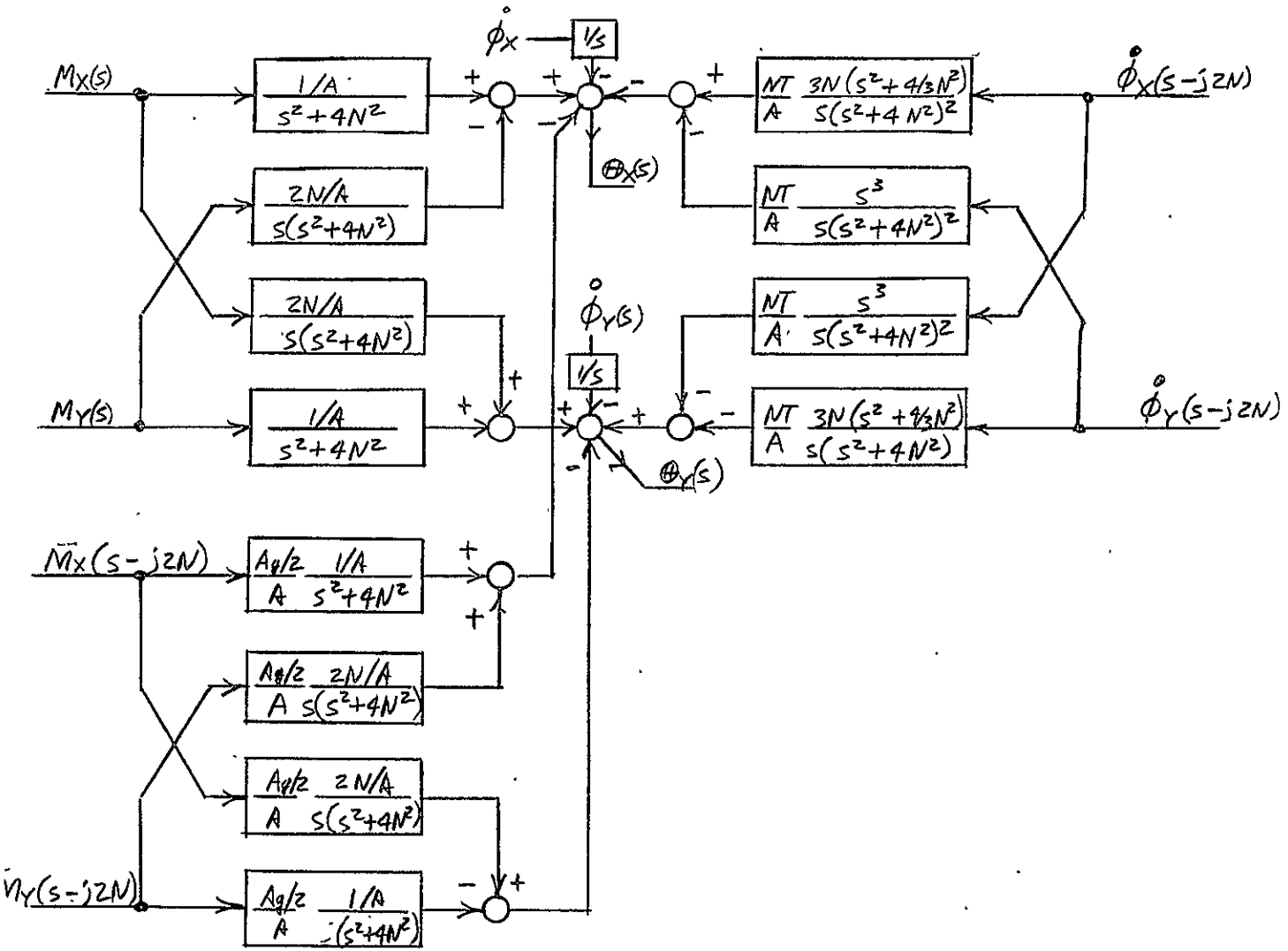

Figure 2-9. Block Diagram of Tuned Gyro Dynamics - Including 2N Components

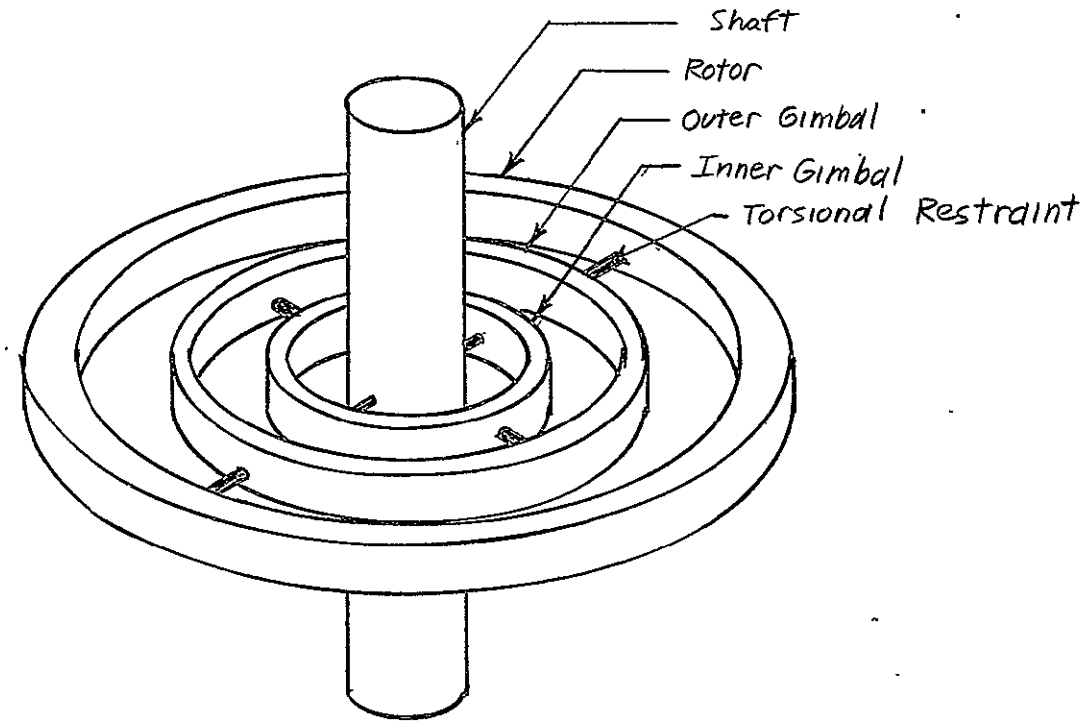

Figure 2-10. A Two Gimbal Gyro

(x_{g2}, y_{g2}, z_{g2}) ----- Fixed in the outer gimbal, with x_{g2} along the outer restraint axis and y_{g2} along the gimbal to gimbal restraint,

also, the system for the inner gimbal is now designated by

(x_{g1}, y_{g1}, z_{g1}) ----- Fixed in the inner gimbal, with x_{g1} along the inner restraint and y_{g1} along the gimbal to gimbal restraint.

Equations (2-2) and (2-8) for shaft and rotor velocities are valid for the two gimbal gyro. Following the development of (2-12), for the inner gimbal,

$$\underline{\omega}_{g1} = \begin{bmatrix} \omega_{xg1} \\ \omega_{yg1} \\ \omega_{zg1} \end{bmatrix} = \begin{bmatrix} 1 & 0 & -\theta_{yg1} \\ 0 & 1 & \theta_{xg1} \\ \theta_{yg1} & -\theta_{xg1} & 1 \end{bmatrix} \cdot \begin{bmatrix} \omega_x \\ \omega_y \\ \omega_z \end{bmatrix} + \begin{bmatrix} \dot{\theta}_{xg1} \\ \dot{\theta}_{yg1} \\ \dot{\theta}_{zg1} \end{bmatrix}, \quad (2\text{-}45)$$

while for the outer,

$$\underline{\omega}_{g2} = \begin{bmatrix} \omega_{xg2} \\ \omega_{yg2} \\ \omega_{zg2} \end{bmatrix} = \begin{bmatrix} 1 & 0 & -\theta_{yg2} \\ 0 & 1 & \theta_{xg2} \\ \theta_{yg2} & -\theta_{xg2} & 1 \end{bmatrix} \cdot \begin{bmatrix} \omega_x \\ \omega_y \\ \omega_z \end{bmatrix} + \begin{bmatrix} \dot{\theta}_{xg2} \\ \dot{\theta}_{yg2} \\ \dot{\theta}_{zg2} \end{bmatrix}. \quad (2\text{-}46)$$

Referring to Figure 2-11, if the restraints from gimbal two to the rotor have the same restoring torque as those between gimbal one and the shaft, the angular deflection of the gimbals about the x-axis is one-half that of the rotor. About the y-axis, the inner gimbal has no deflection, while the outer experiences full rotor deflection. Consequently, for the inner gimbal:

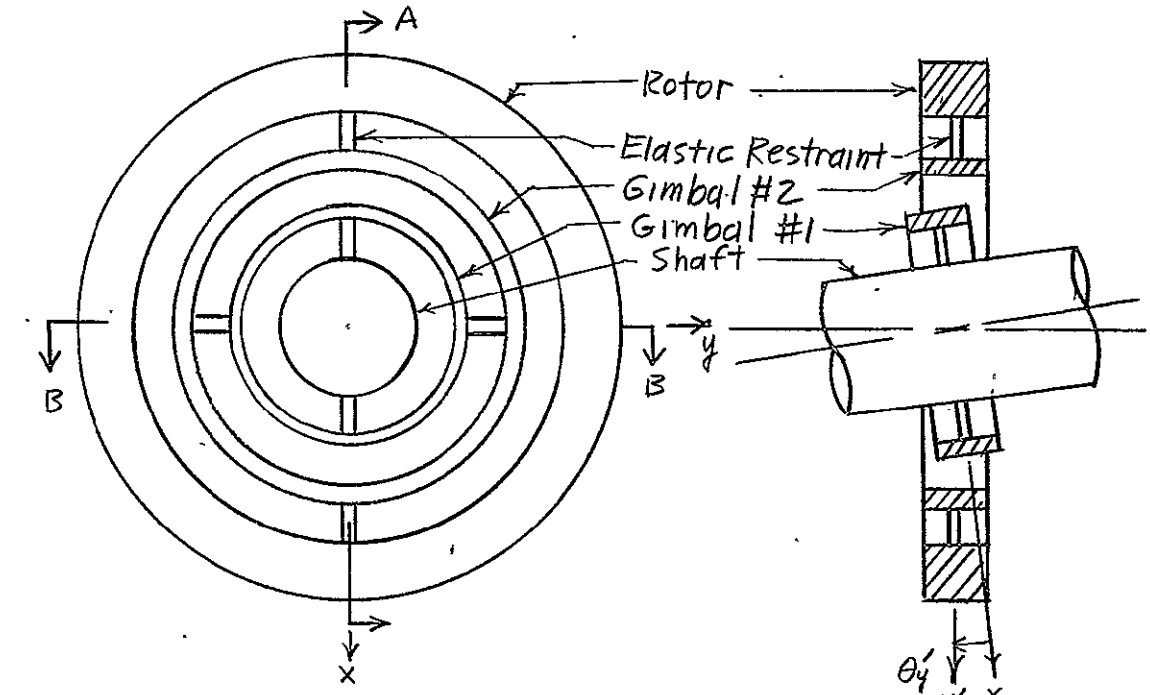

A. Top

B. Right

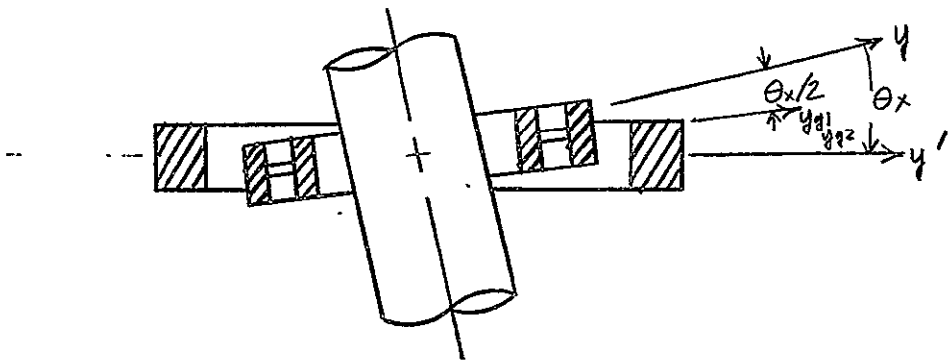

C. Front

Figure 2-11. Relative Deflections of Gimbals and Rotor

$$\left.\begin{aligned} \theta_{xg1} &= \theta_x/2 \\ \dot{\theta}_{xg1} &= \dot{\theta}_x/2 \\ \theta_{yg1} &= \dot{\theta}_{yg1} = 0 \\ \dot{\theta}_{zg1} &\simeq 0 \end{aligned}\right\} \quad (2\text{-}47)$$

and (2-45) becomes

$$\underline{\omega}_{g1} = \begin{bmatrix} \omega_{xg1} \\ \omega_{yg1} \\ \omega_{zg1} \end{bmatrix} = \begin{bmatrix} \omega_x + \dot{\theta}_x/2 \\ \omega_y + N\theta_x/2 \\ N \end{bmatrix} \quad (2\text{-}48)$$

while for the outer gimbal,

$$\left.\begin{aligned} \theta_{xg2} &= \theta_x/2 \\ \dot{\theta}_{xg2} &= \dot{\theta}_x/2 \\ \theta_{yg2} &= \theta_y \\ \dot{\theta}_{yg2} &= \dot{\theta}_y \\ \dot{\theta}_{zg2} &\simeq 0 \ , \end{aligned}\right\} \quad (2\text{-}49)$$

and (2-46) becomes

$$\underline{\omega}_{g2} = \begin{bmatrix} \omega_{xg2} \\ \omega_{yg2} \\ \omega_{zg2} \end{bmatrix} = \begin{bmatrix} \omega_x - N\theta_y + \dot{\theta}_x/2 \\ \omega_y + N\theta_x/2 + \dot{\theta}_y \\ N \end{bmatrix} \quad (2\text{-}50)$$

Figure 2-12 A, B, and C shows free-body-diagrams of the inner gimbal, outer gimbal, and rotor, respectively, of the two gimbal gyro, used to derive the moment equations of the rotor. The moments of inertia about the respective x, y, and z axes are designated A, B, and C, while the subscripts 1 and 2 denote inner and outer gimbals, with

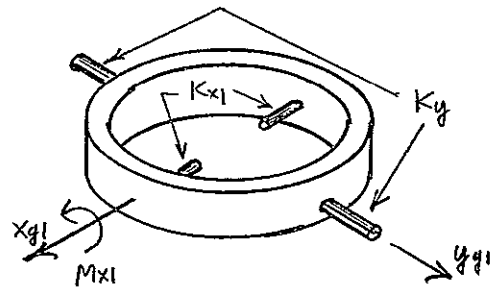

A_1, B_1, C_1 -- Moments of Inertia about x_{g1}, y_{g1}, z_{g1}

A. Inner Gimbal

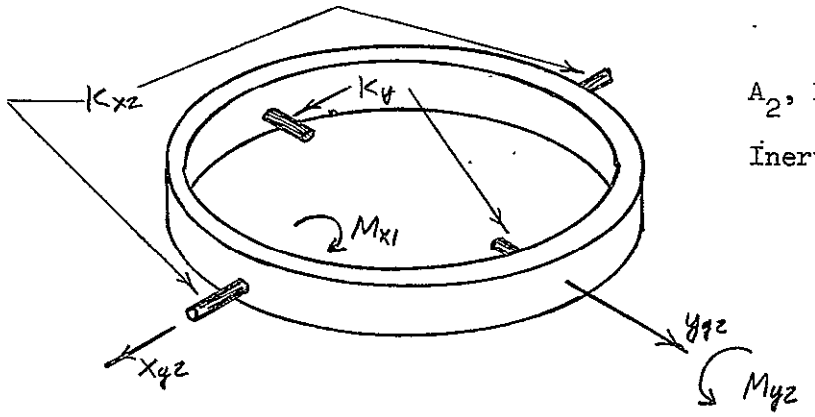

A_2, B_2, C_2 -- Moments of Inertia about x_{g2}, y_{g2}, z_{g2}

B. Outer Gimbal

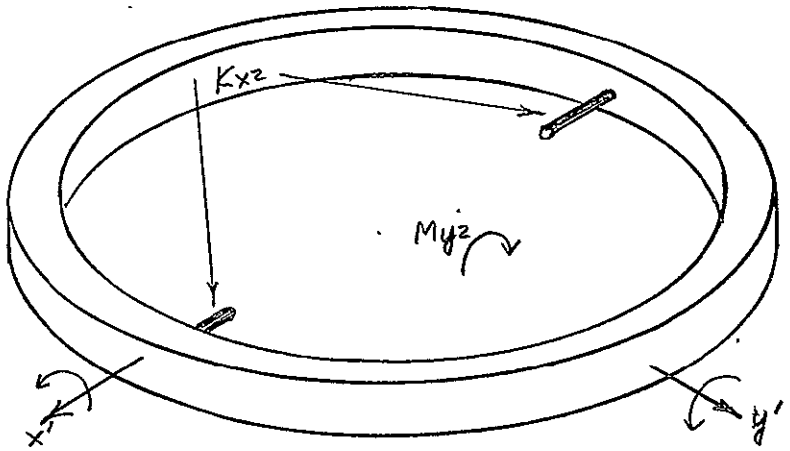

A, B, C -- Moments of Inertia about x´, y´, z´

C. Rotor

Figure 2-12. Free-Body-Diagrams for Two Gimbal Gyros

no subscript for the rotor. The inner and outermost restraint torsional spring constants are K_{x1} and K_{x2}, while that of the middle restraint is K_y. Viscous damping coefficients are defined in a similar manner.

From Figure 2-12a, the moment equation about the x_{g1} axis is

$$M_{x1} = A_1\dot{\omega}_{xg1} + (C_1 - B_1)\,\omega_{yg1}\omega_{zg1} + K_{x1}\theta_{xg1} + D_{x1}\dot{\theta}_{xg1} , \qquad (2\text{-}51)$$

where M_{x1} is the moment delivered from outer to inner gimbal via the middle restraints, which have zero bending. Consequently, for the outer gimbal, Figure 2-12b, the moment equations about x_{g2} and y_{g2} are

$$\left.\begin{aligned} -M_{x1} &= A_2\dot{\omega}_{xg2} + (C_2 - B_2)\omega_{yg2}\omega_{zg2} + K_{x2}(\theta_{xg2} - \theta_{x'}) \\ &\quad + D_{x2}(\dot{\theta}_{xg2} - \dot{\theta}_{x'}) , \\ \text{and} \\ M_{y2} &= B_2\dot{\omega}_{yg2} - (C_2 - A_2)\omega_{xg2}\omega_{zg2} + K_y(\theta_{yg2} - \theta_{ygl}) \\ &\quad + D_y(\dot{\theta}_{yg2} - \dot{\theta}_{ygl}) , \end{aligned}\right\} \qquad (2\text{-}52)$$

respectively, where M_{y2} is a bending moment from the rotor through the outer restraints. For the rotor, from Figure 2-12c, the moment equations are

$$\left.\begin{aligned} M_{x'} &= A\dot{\omega}_{x'} + (C - B)\omega_{y'}\omega_{z'} + K_{x2}(\theta_{x'} - \theta_{xg2}) \\ &\quad + D_{x2}(\dot{\theta}_{x'} - \dot{\theta}_{xg2}) + T_D \sin\theta_{y'} , \\ \text{and} \\ M_{y'} - M_{y2} &= B\dot{\omega}_{y'} - (C - A)\,\omega_{x'}\omega_{z'} , \end{aligned}\right\} \qquad (2\text{-}53)$$

about the x' and y' axes. Equations (2-51) and (2-52) may be combined with (2-53) to give

$$
\left.
\begin{aligned}
M_{x'} &= A\dot{\omega}_{x'} + (C - B)\omega_{y'}\omega_{z'} + A_2\dot{\omega}_{xg2} + (C_2 - B_2)\omega_{yg2}\omega_{zg2} \\
&\quad + A_1\dot{\omega}_{xg1} + (C_1 - B_1)\omega_{yg1}\omega_{zg1} + K_{x1}\theta_{xg1} + D_{x1}\dot{\theta}_{xg1} \\
M_{y'} &= B\dot{\omega}_{y'} - (C - A)\omega_{x'}\omega_{z'} + B_2\dot{\omega}_{yg2} - (C_2 - A_2)\omega_{xg2}\omega_{zg2} \\
&\quad + K_y(\theta_{yg2} - \theta_{yg1}) + D_y(\dot{\theta}_{yg2} - \dot{\theta}_{yg1}) \ .
\end{aligned}
\right\} \quad (2\text{-}54)
$$

Using (2-47) and (2-49), and the small angle approximation which allows $M_{x'} \simeq M_x$ and $M_{y'} \simeq M_y$, (2-52) becomes

$$
\left.
\begin{aligned}
M_x &= A\dot{\omega}_{x'} + (C - B)\omega_{y'}\omega_{z'} + A_1\dot{\omega}_{xg1} + (C_1 - B_1)\omega_{yg1}\omega_{zg1} \\
&\quad + A_2\dot{\omega}_{xg2} + (C_2 - B_2)\omega_{yg2}\omega_{zg2} + K_{x1}\theta_x/2 + D_{x1}\dot{\theta}_x/2 \\
M_y &= B\dot{\omega}_{y'} - (C - A)\omega_{x'}\omega_{z'} + B_2\dot{\omega}_{yg2} - (C_2 - A_2)\omega_{xg2}\omega_{zg2} \\
&\quad + K_y\theta_y + D_y\dot{\theta}_y - T_D\theta_x \ .
\end{aligned}
\right\} \quad (2\text{-}55)
$$

Now, substitute (2-8), (2-48) and (2-50) into (2-54) to get the rotor moment equation in terms of shaft velocities

$$
\left.
\begin{aligned}
M_x &= A(\dot{\omega}_x + \ddot{\theta}_x - N\dot{\theta}_y) + (C - B)\,(\omega_y + \dot{\theta}_y + N\theta_x)\,N + \\
&\quad A_1(\dot{\omega}_x + \ddot{\theta}_x/2) + (C_1 - B_1)\,(\omega_y + N\theta_x/2)\,N + \\
&\quad A_2(\dot{\omega}_x - N\dot{\theta}_y + \ddot{\theta}_x/2) + (C_2 - B_2)\,(\omega_y + N\theta_x/2 + \dot{\theta}_y)\,N + \\
&\quad K_{x1}\cdot\theta_x/2 + D_{x1}\cdot\dot{\theta}_x/2 + T_D\theta_y \\
M_y &= B(\dot{\omega}_y + \ddot{\theta}_y + N\dot{\theta}_x) - (C - A)\,(\omega_x + \dot{\theta}_x - N\theta_y) + \\
&\quad B_2(\dot{\omega}_y + N\dot{\theta}_x/2 + \ddot{\theta}_y) - (C_2 - A_2)\cdot \\
&\quad (\omega_x - N\theta_y + \dot{\theta}_x/2)\,N + K_y\theta_y + D_y\dot{\theta}_y - T_D\dot{\theta}_y \ .
\end{aligned}
\right\} \quad (2\text{-}56)
$$

Collecting terms in (2-56) gives

$$
\begin{aligned}
M_x = {} & \ddot{\theta}_x[A + (A_1 + A_2)/2] + \dot{\theta}_x D_{x1}/2 \\
& \theta_x\{N^2[C - B + (C_1 - B_1 + C_2 - B_2)1/2] + K_{x1}/2\} \\
& \dot{\theta}_y N(C - A - B + C_2 - A_2 - B_2) + \theta_y T_D + \\
& \dot{\omega}_x(A + A_1 + A_2) + \omega_y N[C - B + C_1 - B_1 + C_2 - B_2] \\
M_y = {} & \ddot{\theta}_y[B + B_2] + \dot{\theta}_y D_y + \theta_y\{N^2(C - A + C_2 - A_2) + K_y\} - \\
& \dot{\theta}_x N(C - A - B + C_2/2 - A_2/2 - B_2/2) - \\
& \theta_x T_D + \dot{\omega}_y(B + B_2) - \omega_x N\ (C - A + C_2 - A_2),
\end{aligned}
\qquad (2\text{-}57)
$$

which are the coupled differential equations of motion in shaft fixed coordinates for the rotor of a two-gimbal gyro.

Complex Transformation

Proceeding as before, the symmetrical components are defined

$$
\begin{aligned}
I &= [A + B + (A_1 + A_2)/2 + B_2]/2 \\
I' &= [A - B + (A_1 + A_2)/2 - B_2]/2 \\
D &= [D_{x1}/2 + D_y]/2 \\
D' &= [D_{x1}/2 - D_y]/2 \\
K &= [K_{x1}/2 + K_y]/2 \\
K' &= [K_{x1}/2 - K_y]/2 \\
J &= (2C - B - A\ 3C_2/2 + C_1/2 - B_1/2 - B_2/2 - A_2)/2 \\
J' &= [- B - A - (B_1 + B_2 + C_1 + C_2)/2 + A_2]/2 \\
L &= [2(C - A - B) + 3(C_2 - A_2 - B_2)/2]/2 \\
L' &= (C_2 - A_2 - B_2)/4
\end{aligned}
\qquad (2\text{-}58)
$$

$$\left.\begin{aligned} P &= (A + B + A_1 + A_2 + B_2)/2 \\ P' &= (A - B + A_1 + A_2 - B_2)/2 \\ R &= (2C - A - B + 2C_2 + C_1 - B_1 - B_2 - A_2)/2 \\ R' &= (A - B + C_1 - B_1 - B_2 + A_2)/2 \end{aligned}\right]$$

These symmetrical components (2-58) are substituted into (2-57) to give the rotor moment equation in terms of symmetrical components, which is identical symbolically to (2-21), only the components are defined differently in (2-58). As in the single gimbal case, (2-21) is combined into a single equation using complex notation, transformed to the case-fixed coordinate system, and Laplace transformed to give (2-28). The coefficients of variables, $Z_1(s)$, $Z_2(s)$, etc., are defined in (2-24) and substituted into (2-28) to give

$$\begin{aligned} &Z_1(s)\theta_{XY}(s) + Z_2(s)\bar{\theta}_{XY}(s - j2N) = M_{XY}(s) - \\ &Z_3(s)\dot{\phi}_{XY}(s) - Z_4(s)\dot{\bar{\phi}}_{XY}(s - j2N), \end{aligned} \tag{2-30}$$

which is manipulated to give a conjugate equation at twice spin frequency,

$$\begin{aligned} &\bar{Z}_1(s - j2N)\bar{\theta}_{XY}(s - j2N) + \bar{Z}_2(s - j2N)\bar{\theta}_{XY}(s) = \bar{M}_{XY}(s - j2N) \\ &-\bar{Z}_3(s - j2N)\dot{\bar{\phi}}_{XY}(s - j2N) - \bar{Z}_4(s - j2N)\bar{\phi}_{XY}(s) . \end{aligned} \tag{2-31}$$

Simultaneous solution of (2-30) and (2-31) yield

$$\begin{aligned} \begin{bmatrix} \theta_{XY}(s) \\ \bar{\theta}_{XY}(s - j2N) \end{bmatrix} &= \begin{bmatrix} Z_1(s) & Z_2(s) \\ \bar{Z}_2(s - j2N) & Z_1(s - j2N) \end{bmatrix}^{-1} \cdot \begin{bmatrix} M_{XY}(s) \\ \bar{M}_{XY}(s - j2N) \end{bmatrix} \\ &- \begin{bmatrix} Z_3(s) & Z_4(s) \\ \bar{Z}_4(s - j2N) & Z_3(s - j2N) \end{bmatrix} \cdot \begin{bmatrix} \dot{\phi}_{XY}(s) \\ \dot{\bar{\phi}}_{XY}(s - j2N) \end{bmatrix} . \end{aligned} \tag{2-32}$$

Again the simplifying assumptions of

1. Negligable drag and damping, therefore

$$T_D = D = D' = D_R = 0$$

2. Symmetry, $A = B$, $A_1 = B_1$, $A_2 = B_2$, and

$$K_{x1} = K_{x2} = K_y = k$$

allow us to evaluate (2-32) by simplifying (2-58) which becomes

$$\begin{aligned}
I &= A + A_1/4 + 3\,A_2/4 \\
I' &= A_1/4 - A_2/4 \\
K &= 3/4\,k \\
K' &= -\,1/4\,k \\
J &= C - A + 3\,C_3/4 - C_1/4 - A_1/4 - 3\,A_2/4 \\
J' &= (C_1 - C_2 - A_1 + A_2)/4 \\
L &= C - 2\,A + 3\,C_2/4 - 3\,A_2/2 \\
L' &= C_2/4 - A_2/2 \\
P &= A + A_1/2 + A_2 \\
P' &= A_1/2 \\
R &= C - A + C_2 + C_1/2 - A_1/2 - A_2 \\
R' &= C_1/2 - A_1/2
\end{aligned} \qquad (2\text{-}59)$$

which may in turn be used in (2-29) to obtain

$$
\left.
\begin{aligned}
Z_1(s) &= s^2(A + A_1/4 + 3A_2/4) - j2Ns\,(C/2 + 3C_2/8 \\
&\quad + A_1/4) + (3/4)k - N^2(A_1/2 - C_1/4) \\
Z_2(s) &= s^2(A_1 - A_2)/4 - jNs(A_1/2 - C_2/4) - k/4 \\
&\quad - N^2(A_1/2 - C_1/4) \\
Z_3(s) &= s(A + A_1/2 + A_2) - jN(C + C_1/2 + C_2) \\
Z_4(s) &= sA_1/2 - jN(A_1 - C_1/2) \quad .
\end{aligned}
\right\} \quad (2\text{-}60)
$$

Conjugation and substitution of $s - j2N$ for s in (2-60) gives

$$
\left.
\begin{aligned}
\overline{Z}_1(s - j2N) &= s^2(A + A_1/4 + 3A_2/4) - j2Ns(2A - C/2 \\
&\quad + A_1/4 + 3A_2/2 - 3C_2/8) + (3/4)k - N^2[4A - 2C + A_1/2 \\
&\quad + 3A_2 - 3C_2/2 - C_1/4] \\
\overline{Z}_2(s - j2N) &= s^2(A_1 - A_2)/4 - jNs(A_1/2 - A_2 + C_2/4) - k/4 \\
&\quad - N^2(A_1/2 - A_2 - C_1/4 + C_2/2) \\
\overline{Z}_3(s - j2N) &= s(A + A_1/2 + A_2) - jN(2A - C + A_1 - C_1/2 - C_2) \\
\overline{Z}_4(s - j2N) &= sA_1/2 - jNC_1/2
\end{aligned}
\right\} \quad (2\text{-}61)
$$

Transfer Function

The transfer function for the two gimbal gyro may be found by using

$$
\begin{aligned}
\theta_{XY}(s) = \{&\overline{Z}_1(s - j2N)M_{XY}(s) - Z_2(s)\overline{M}_{XY}(s - j2N) \\
&-[\overline{Z}_1(s - j2N)Z_3(s) - Z_2(s)\overline{Z}_4(s - j2N)]\phi_{XY}(s) \\
&-[\overline{Z}_1(s - j2N)Z_4(s) - Z_2(s)Z_3(s - j2N)]\overline{\phi}_{XY}(s - j2N)\} \\
&/[Z_1(s) \cdot \overline{Z}_1(s - j2N) - Z_2(s) \cdot \overline{Z}_2(s - j2N)], \quad (2\text{-}36)
\end{aligned}
$$

along with (2-60) and (2-61). The approximation used is that rotor inertias are large compared with gimbal inertias. The constant term of the characteristic equation, $Z_1(s) \cdot \overline{Z}_1(s - j2N) - Z_2(s) \cdot Z_2(s - j2N)$, is

$$\begin{aligned}&[3/4k - N^2(A_1/2 - C_1/4)] \cdot [3/4k - N^2(4A - 2C + A_1/2 + 3A_2 \\ &- 3C_2/2 - C_1/4] - [-k/4 - N^2(A_1/2 - C_1/4)] \cdot [-k/4 \\ &- N^2(A_1/2 - C_1/4 - A_2 + C_2/4)]\end{aligned} \tag{2-63}$$

which is forced to zero. It is expedient to do this in the following manner:

1. Make the constant term of $Z_1(s)$ equal zero. This removes rotor inertias from the tuning condition, allowing the designer independent choice or rotor and suspension characteristics.

2. Make the constant term of $\overline{Z}_2(s - j2N)$ equal zero, completing the tuning procedure.

Thus

$$\left.\begin{aligned}&3/4k - N^2(A_1/2 - C_1/4) = 0, \\ \text{and} \\ &k/4 - N^2(A_2 - C_2/2 - A_1/2 + C_1/4) = 0,\end{aligned}\right\} \tag{2-64}$$

which may be realized if

$$A_2 - C_2/2 - 2A_1/3 + C_1/3 = 0 \tag{2-65}$$

one solution of which is

$$A_2 = 2/3A_1, \quad C_2 = 2/3C_1 \tag{2-66}$$

Equation (2-36) may now be written

$$\theta_{xy}(s) = \frac{M_{XY}(s)}{Z_1(s)} - \frac{Z_2(s)}{Z_1(s - j2N)Z_1(s)} \overline{M}_{XY}(s - j2N) - \frac{Z_3(s)}{Z_1(s)} \dot{\phi}_{XY}(s) \left[\frac{Z_4(s)}{Z_1(s)} - \frac{Z_2(s)}{Z_1(s)} \frac{\overline{Z}_3(s - j2N)}{\overline{Z}_1(s - j2N)} \right] \dot{\overline{\phi}}_{XY}(s - j2N) \tag{2-67}$$

as the tuned transfer function. Under this condition

$$Z_1(s) = s^2A - j2NsA$$

$$Z_1(s) \cdot \overline{Z}_1(s - j2N) = A^2s^2(s - j2N)^2$$

$$Z_3(s) = sA - j2NA$$

$$Z_3(s)/Z_1(s) = 1/s$$

$$\overline{Z}_3(s - j2N)/\overline{Z}_1(s - j2N) = 1/(s - j2N)$$

and the transfer function becomes

$$\Theta_{XY}(s) = \frac{M_{XY}(s)}{sA(s - j2N)} - \frac{A_1/12}{A^2} \cdot \frac{\overline{M}_{XY}(s - j2N)}{s(s - j2N)} - \frac{\dot{\phi}_{XY}(s)}{s} - \frac{5}{12} \frac{A_1}{A} \frac{\dot{\overline{\phi}}_{XY}(s - j2N)}{(s - j2N)} \tag{2-68}$$

Separating (2-68) into its real and imaginary component

$$\left.\begin{aligned} \Theta_X(s) = {} & \frac{sM_X(s)}{As(s^2 + 4N^2)} - \frac{2N \cdot M_Y(s)}{As(s^2 + 4N^2)} - \frac{\dot{\phi}_X(s)}{s} \\ & - \frac{A_1/12}{A^2} \cdot \frac{sM_X(s - j2N) + 2N \cdot M_Y(s - j2N)}{s(s^2 + 4N^2)} \\ & - \frac{5}{12} \cdot \frac{A_1}{A} \cdot \frac{s\dot{\overline{\phi}}_X(s - j2N) + 2N \cdot \dot{\overline{\phi}}_Y(s - j2N)}{(s^2 + 4N^2)} \end{aligned}\right\} \tag{2-69}$$

$$\theta_\gamma(s) = \frac{2N \cdot M_X(s)}{As(s^2 + 4N^2)} + \frac{sM_X(s)}{As(s^2 + 4N^2)} - \frac{\dot{\phi}_Y(s)}{s}$$

$$- \frac{A_1/12}{A^2} \cdot \frac{2NM_X(s - j2N) - sM_X(s - j2N)}{s(s^2 + 4N^2)}$$

$$- \frac{5}{12} \cdot \frac{A_1}{A} \cdot \frac{2N \cdot \dot{\phi}_X(s - j2N) - s\dot{\phi}_Y(s - j2N)}{(s^2 + 4N^2)}$$

The transfer function for direct rate inputs, and moment inputs, both direct and 2N is similar to that of the single gimbal gyro (2-44), differing only in the scale factor of the 2N moment input. A constant angular displacement at 2N (impulse of rate) is not rectified, which improves the quality of the gyro as a rate integrating sensor.

V. COMPARISON OF ONE AND TWO GIMBAL GYRO DYNAMICS

The transfer function for direct rate and moment inputs, which is required by the system designer to use the gyro as a strapdown instrument, is identical for both the single and two gimbal gyros. The principle differences are (1) elimination of the undesirable 2N rectification effect, and (2) a tuning condition, (2-64), which is independent of rotor inertias, in the two gimbal gyro. Both of these characteristics are important. The 2N rectification in a single gimbal gyro destroys its usefulness as a high quality attitude sensor. A tuning condition which contains rotor inertias (2-40) means that the dynamic antispring is not a function of gimbal inertias and speed alone, consequently, the rotor cannot be considered free, the requirement of a high quality rate integrating gyro. This lack of freedom is displayed in the 2N rectification of the single gimbal gyro. The conclusion which may be reached here is that a tuned gyro must have more than one gimbal for successful operation as a sensor.

CHAPTER III

REBALANCE LOOP ANALYSIS FOR A DRY, TUNED, TDF GYRO

For strapdown applications, the plant dynamics derived for the gyro of the preceeding chapter must be included in a closed loop. This loop causes the gyro to be a null instrument, any sensed deviation of the rotor position with respect to the case from null causes an applied restoring or rebalance torque to force the rotor back to null. As in the case of the SDF gyro, the torquer current can be measured to give an indication of sensor motion. The plant dynamics, including torquer coil dynamics and pickoff gain, is shown in Figure 3-1. Both analog and the digital rebalance loops will be investigated.

I. ANALOG LOOPS

For ease of design and hardware implementation, rebalance loops using continuous signals are preferred. Two different analog rebalance loop designs are presented in this section.

Teledyne Loop

The Teledyne design is based on meeting the following criteria:

1. The steady-state output angle (rotor hangoff) errors are zero for constant angular velocity inputs.
2. The maximum absolute transient error is less than 5 milliradians to keep the rotor from hitting its stops.
3. The feedback loop gain must be attenuated at the spin frequency, N, to avoid rectification errors at this frequency.

This design was implemented using the plant transfer function in complex form,

$$\theta_{XY}(s) = \frac{M_{XY}(s)}{As(s - j2N)} - \frac{\dot{\phi}_{XY}(s)}{s} \qquad (2\text{-}38)$$

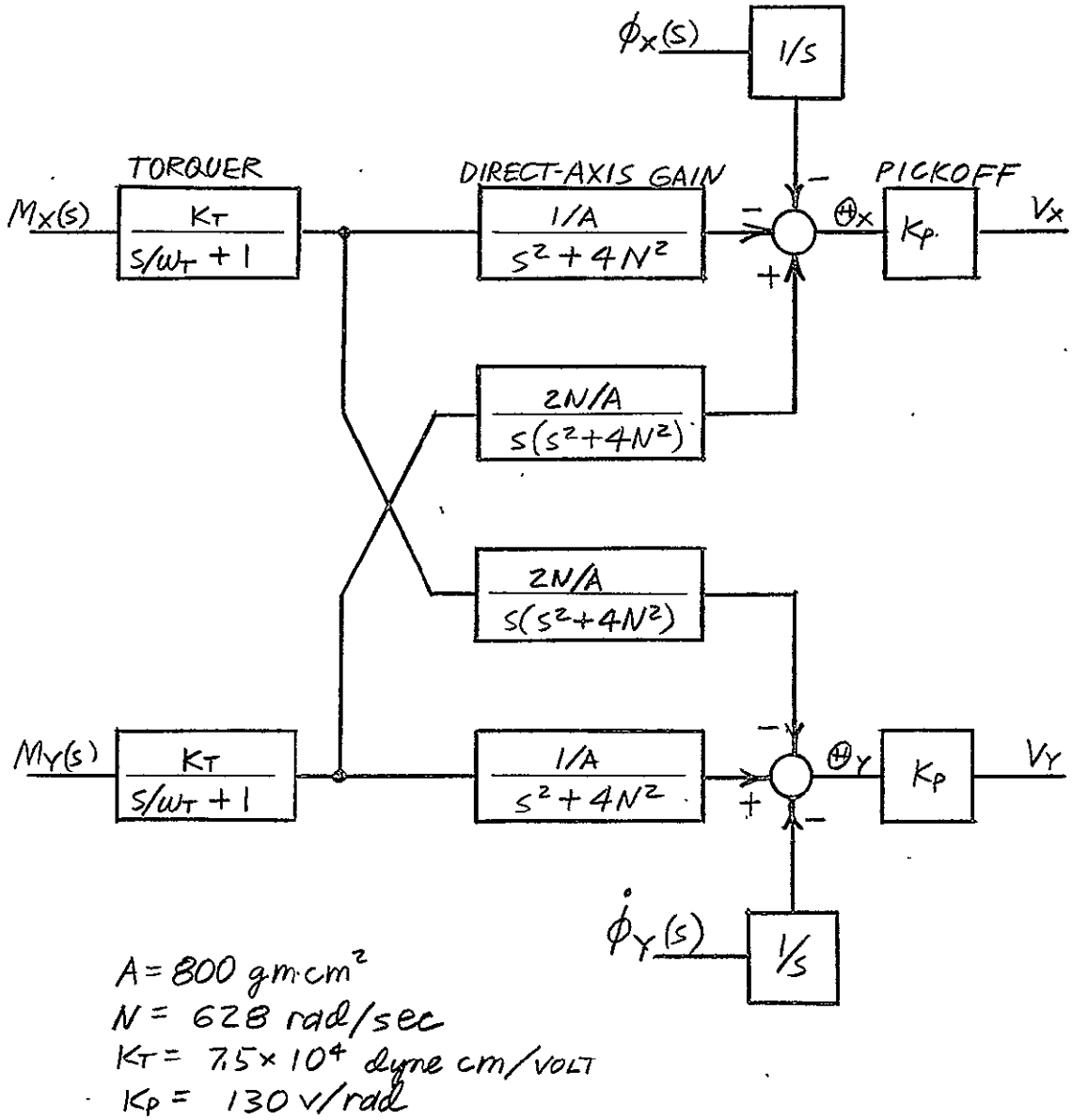

Figure 3-1. Plant Dynamics of Dry Tuned TDF Gyro

A root locus design was used resulting in the rebalance of Figure 3-2, a single loop with the following variables in complex form:

Rate input -------- $\dot{\phi}_{XY}(s)$

Moment input ------ $M_{XY}(s)$

Output (rotor hangoff) angle ------- θ_{XY}

This loop contains physically unrealizable poles and zeros, that is, complex roots which are not accompanied by a conjugate. Using 2-22, which converts the variables in complex form into their real variable components, the feedback component of the loop of Figure 3-2 is transformed to Figure 3-3 in which both direct and cross-coupled terms appear. The general effect of complex roots without conjugates in the complex variable domain is to produce both direct and cross-coupled terms in the real variable domain.

Noninteracting Loop

Another analog rebalance loop uses the well known principle of noninteraction,[9] in which the matrix of the open loop transfer function is diagonalized. This diagonalization causes the closed loop matrix to also be diagonal, which decouples the response of all outputs but one to a given input. Thus, each input is paired with an output, and these input-output pairs are noninteracting with each other. This noninteraction essentially reduces a multi-variable system with n inputs and n outputs to n separate single-input-single-output systems which may be compensated individually using classical techniques.

The simplest method of diagonalizing a matrix, M, is to multiply it by its inverse, M^{-1}, since $MM^{-1} = I$, provided M is non-singular. The plant gain matrix (which excludes the torquers and pickoffs) is

$$G = \frac{1/A}{s^2 + 4N^2} \begin{bmatrix} 1 & -2N/s \\ 2N/s & 1 \end{bmatrix} , \qquad (3\text{-}1)$$

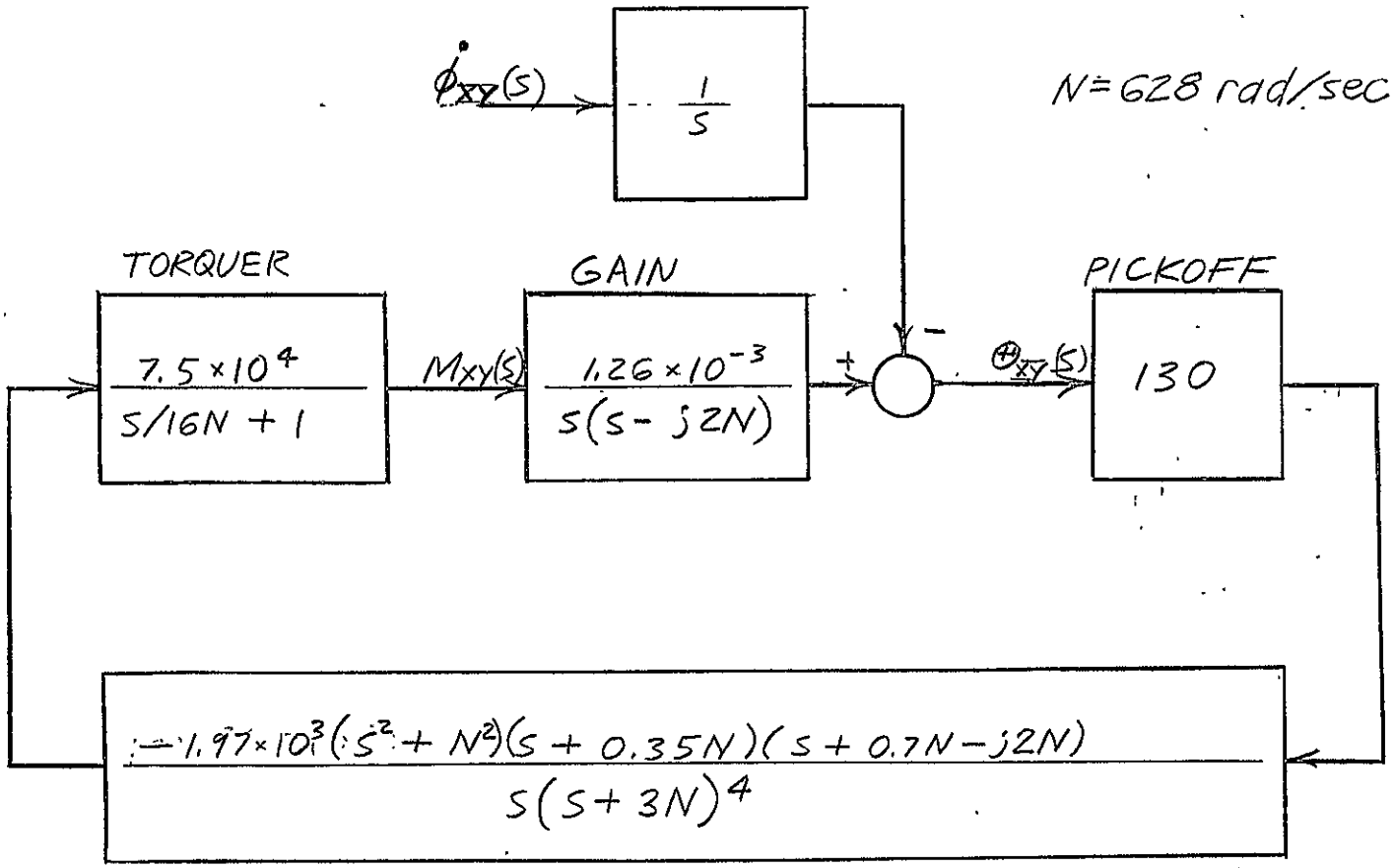

Figure 3-2. Teledyne Rebalance Loop in Complex Coordinate Form

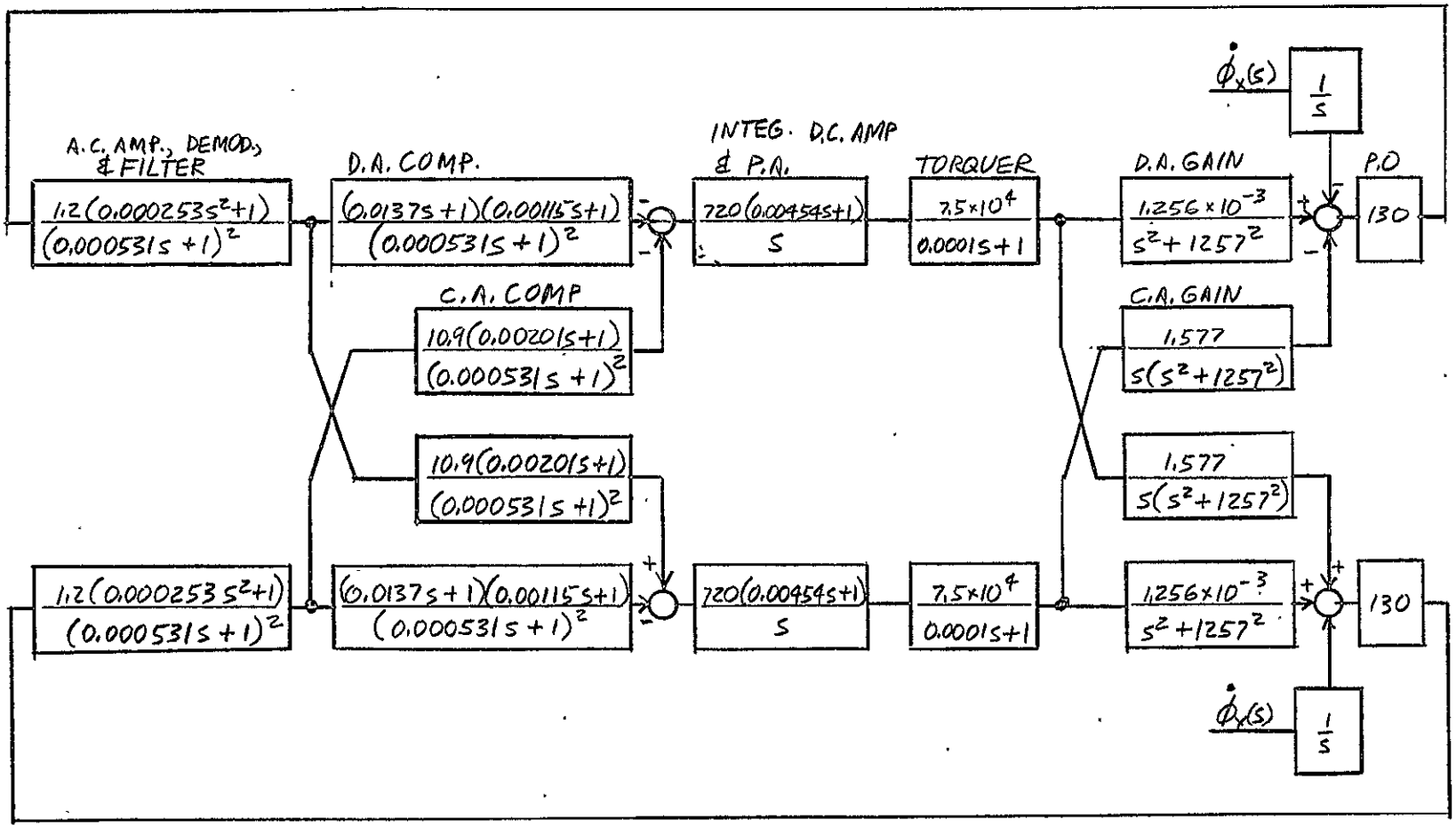

Figure 3-3. Teledyne Analog Rebalance Loop in Realizable Form

which, inverted, becomes

$$G^{-1} = As \cdot \begin{bmatrix} s & 2N \\ -2N & s \end{bmatrix} . \qquad (3\text{-}2)$$

Because of linearity of the system, this inverted plant gain matrix may be placed anywhere within the feedback loop to obtain diagonalization. In addition, each element of this matrix may be divided by s, or s^2, to give a type I, or II, closed loop response, respectively.

In order to compare the performance of the noninteracting loop with that of the Teledyne loop a type II system was designed. The Bode plot of the open loop is shown in Figure 3-4. The gain of 10^5 gives a steady-state error in the rotor hangoff angle of 0.5 milliradian for an acceleration input of 50 rad/sec^2, which is comparable to the Teledyne response. A lead network is used to add a zero at $\omega = 200$ so the slope of the open loop transfer function is -20 db/octave at the zero db crossing. This gives a theoretical 10 to 90 percent rise time of 7.3 msec and a 1.2% overshoot. The additional poles in the transfer function are at $\omega = 10000$ rad for the torquer coil and $\omega = 20000$ rad for the lead network pole. This design permits the addition of a notch filter with imaginary zeros a $\omega = \pm jN$, and two real poles at $\omega = 3N$, $N = 628$ rad, if one is considered necessary. The single-input-single-output transfer function is

$$\frac{\theta_x}{\dot{\phi}_x} = \frac{10^5(s/200 + 1)}{s^2(s/20000 + 1)(s/10000 + 1)} . \qquad (3\text{-}3)$$

Figure 3-5 shows a block diagram of the noninteracting loop used to achieve this transfer function.

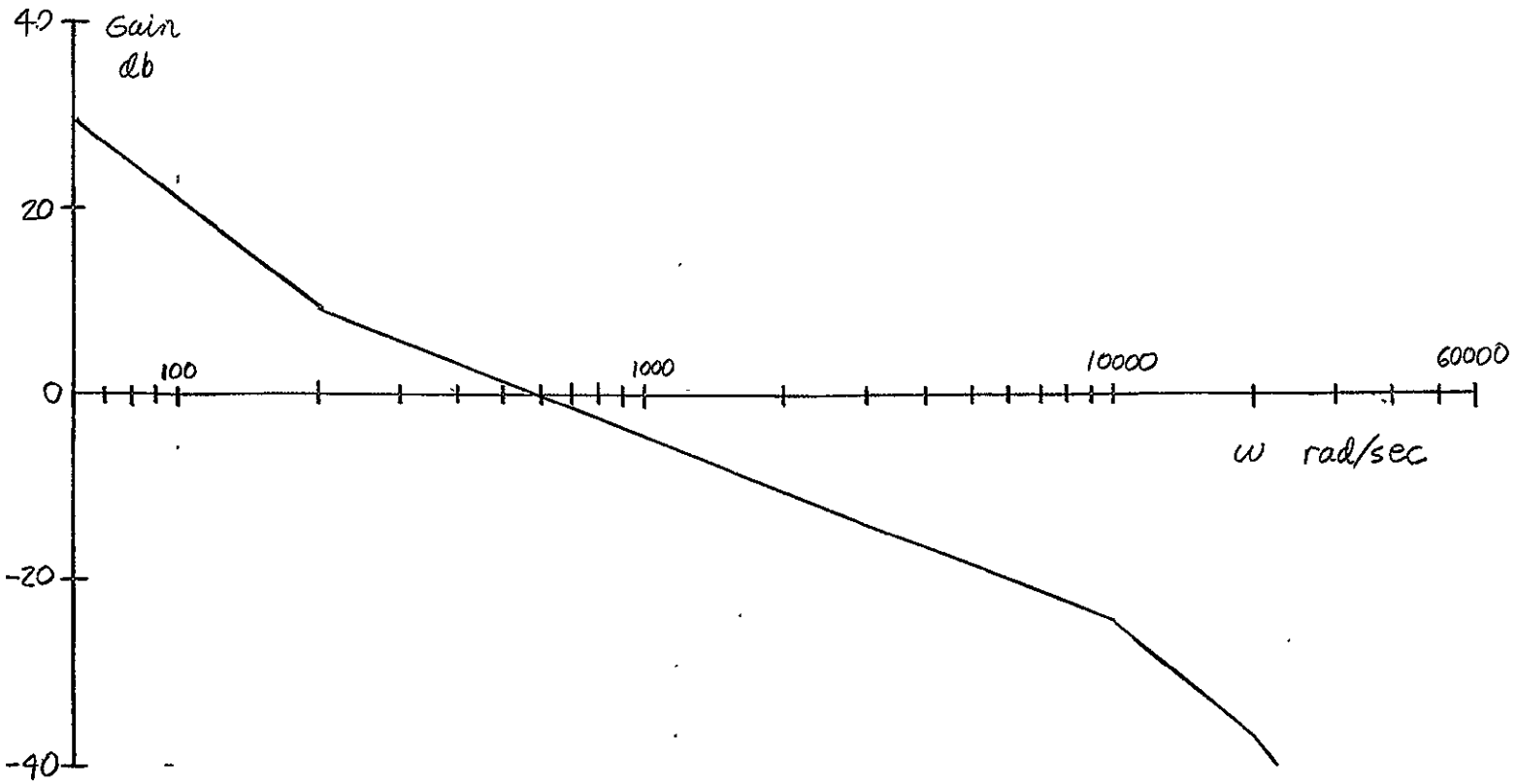

Figure 3-4. Bode Plot of SISO Noninteracting Open Loop

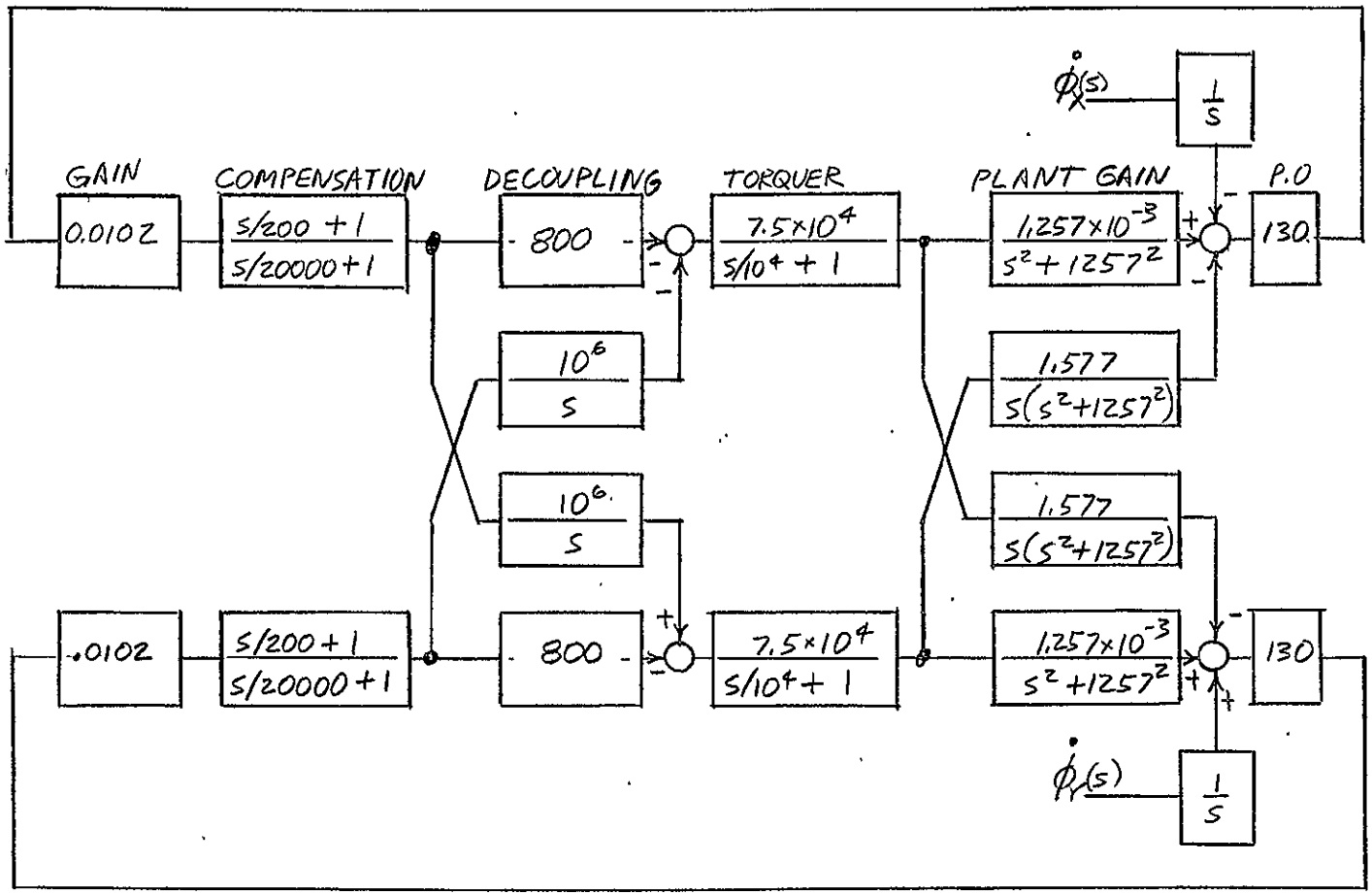

Figure 3-5. Noninteracting Analog Rebalance Loop

Comparison of the Teledyne and Noninteracting Loops and the Results of Simulation

Both the Teledyne and noninteracting designs are satisfactory to rebalance the dry tuned TDF gyro. The Teledyne loop, which in realizable form is a two-input-two-output system, is the more difficult of the design methods to implement. The implementation of this design involves using system variables in the complex coordinate form (Figure 3-2, page 49) which results in a root locus design in which real-axis symmetry does not exist. The notch filter is an essential part of this design; its removal causes the loop to become unstable.

The noninteracting design, which reduces the design problem to that of a single-input-single-output system, has one flaw. The noninteraction depends on exact knowledge of decoupling and plant parameters, in real world problems this never the case. The consequences of this inexact noninteraction are imaginary axis closed loop poles in the vicinity of 2N, and small off-diagonal elements in the transfer matrix, which also contain imaginary closed loop poles near 2N. These poles limit the closed loop bandwidth of the system.

Results of simulation shown in Table 3-1 of the Teledyne loop and the noninteracting loop with a notch filter included shows the Teledyne loop having slightly superior performance.

Table 3-1: Rotor Hangoff Angle for Dry Tuned TDG Gyro with Acceleration Input (x-axis) of 50 rad/sec^2

Rebalance Loop Loop	Rise time 10%-90% msec	5% Settling Time msec	% Overshoot	S.S. Error Millirad
Noninteracting	6.0	21.0	19.2	0.50
Teledyne	6.0	15.0	9.2	0.53

II. DIGITAL REBALANCE

Pulse width modulators (PWM's) may be inserted ahead of the torquers so that the loop may operate in the PTSA mode. From the equal area principle[10], a linear system gives the same response at the time of sampling, regardless of the waveshape of the input, provided the area under the input curve is equal. Thus the current to the torquer may be pulse width modulated without a deterioration of sensor performance.

One type of PWM employed is binary width modulation (BWM), in which the torquer current assumes a constant magnitude of positive or negative polarity, such that the net current time produce (area) over a sampling period is proportional to the input of the BWM at the sampling time. Because constant current is delivered to the torquer coil, its power is constant regardless of the net current; consequently, unstationary thermal gradients in the torquer coils, which can cause scale factor change, are avoided. Data resolution is obtained by varying the positive and negative widths in small discrete steps, as shown in Figure 3-6.

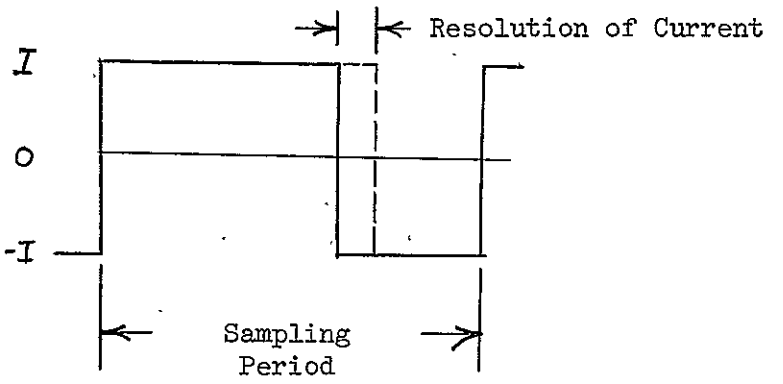

Figure 3-6. BWM Current

Both the Teledyne and noninteracting designs were simulated with BWM's in the loop ahead of the torquer coils (Figures 3-7 and 3-8). The results of these simulations are shown in Figure 3-9 through 3-12 for sampling periods of 0.5 and 0.1 msec. A constant angular acceleration input about the x-axis of 50 rad/sec^2 is used in each case. The x- and y-rotor hangoff angles and inputs to the x- and y-BWM's are plotted.

For a sampling period of 0.5 msec, the Teledyne loop produced objectionably large 500 Hz ripple at the inputs to the BWM's, as well as substantially large transients in the rotor hangoff angles. For the noninteracting loop the inputs to be BWM's are free of ripple, but have constant offsets from the analog case. The rotor hangoff angles have approximately 4 mrad peak-to-peak ripple at 200 Hz. Therefore, binary width modulation with a sampling period of 0.5 msec is considered unsatisfactory for both the Teledyne and noninteracting designs.

For a sampling period of 0.1 msec the Teledyne loop has a small amplitude disturbance of undiscernable low frequency in both the rotor hangoff angles and the inputs to the BWM's. The variables approach the values of those of the case of analog rebalance, and the small amount of deviation is not considered sufficient to degrade sensor performance. The noninteracting loop has a 200 Hz frequency component in the rotor hangoff angles of approximately 0.4 mrad peak-to-peak, which is acceptable. The BWM inputs contain no noticeable deviation from the analog case. For both the Teledyne and noninteracting designs, binary width modulation with a sampling period of 0.1 msec is acceptable.

Existence of Limit Cycles

In designing a PTSA loop, it is desirable to avoid limit cycles, since they can cause signal excursions beyond acceptable limits of operation of the system and can also generate extraneous information regarding sensor motion. This section is devoted to the determination of the existence of limit cycles using a describing function (DF) for

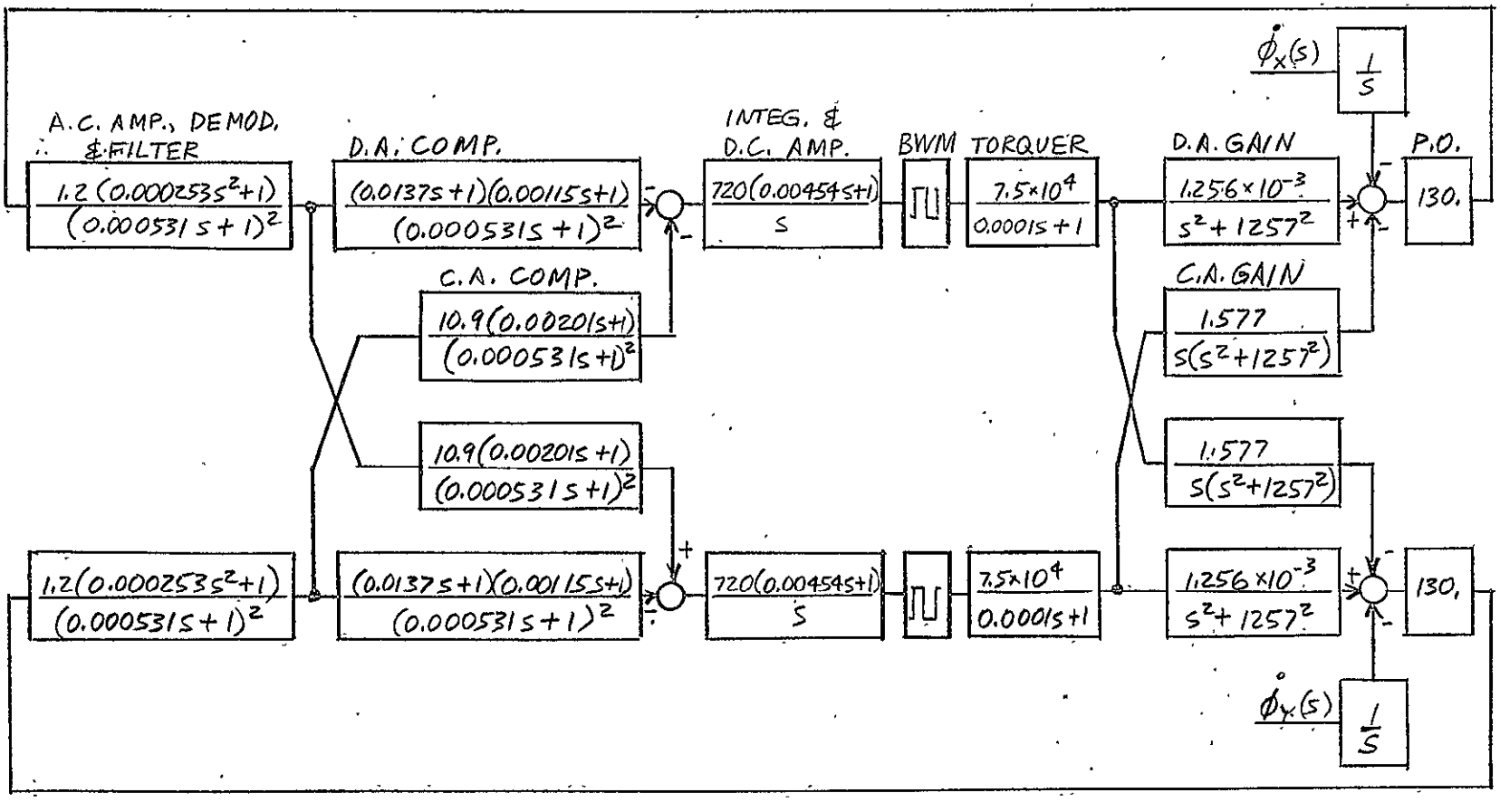

Figure 3-7. Teledyne Rebalance Loop With BWM

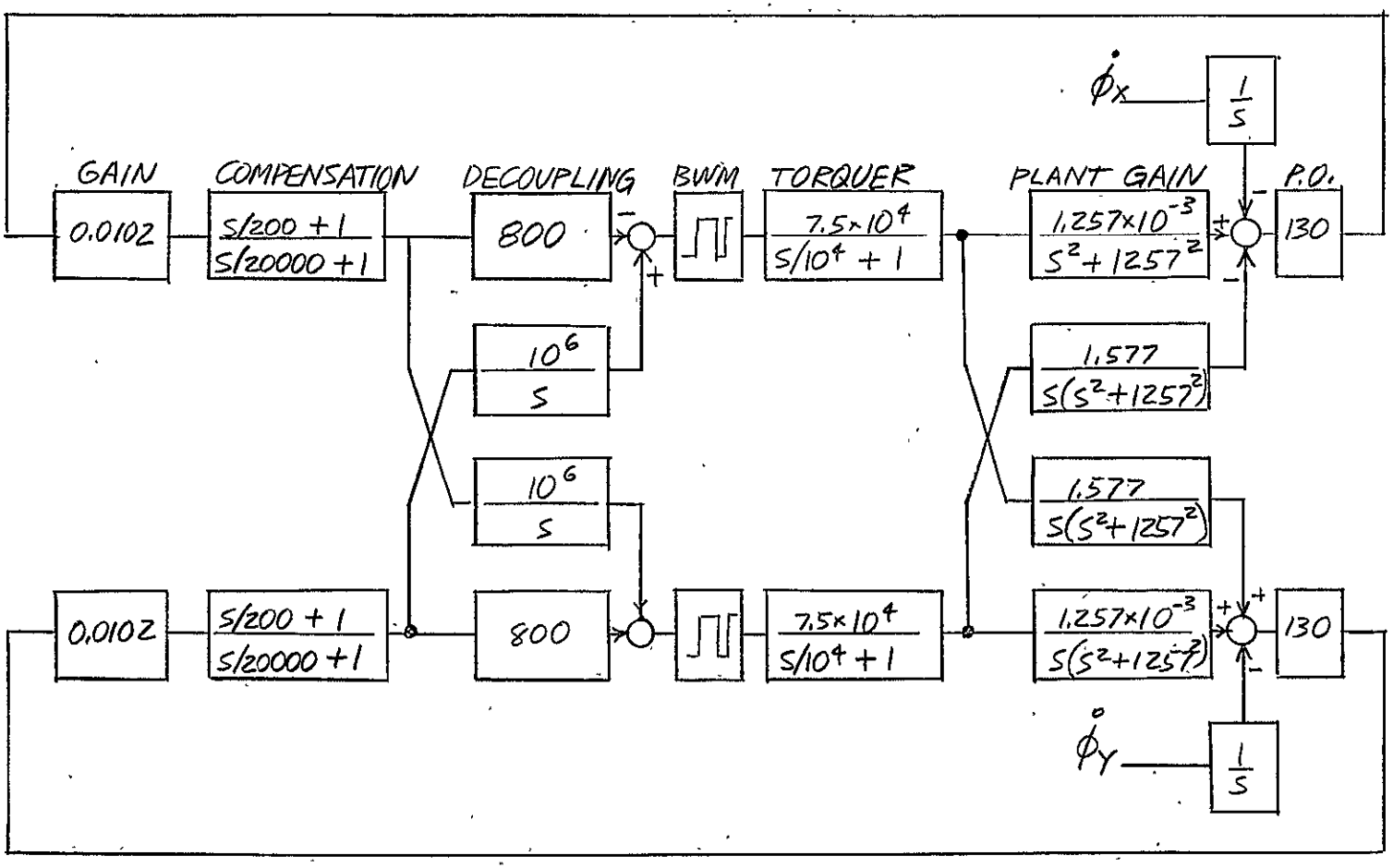

Figure 3-8. Noninteracting Rebalance Loop With BWM

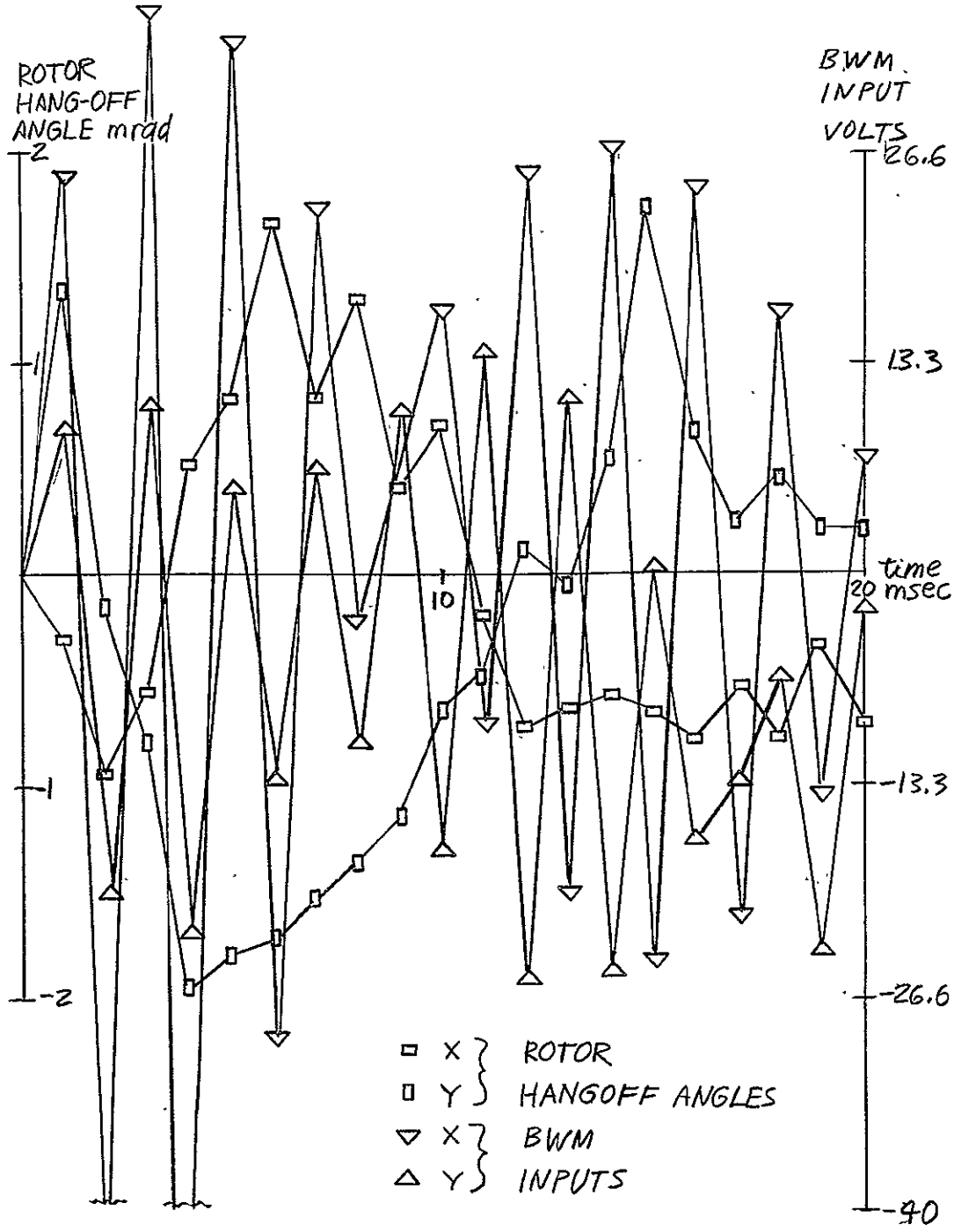

Figure 3-9. Simulation for Digital Teledyne Loop,

Rate Input to X-Axis = 50t, BWM Period = 0.5 msec

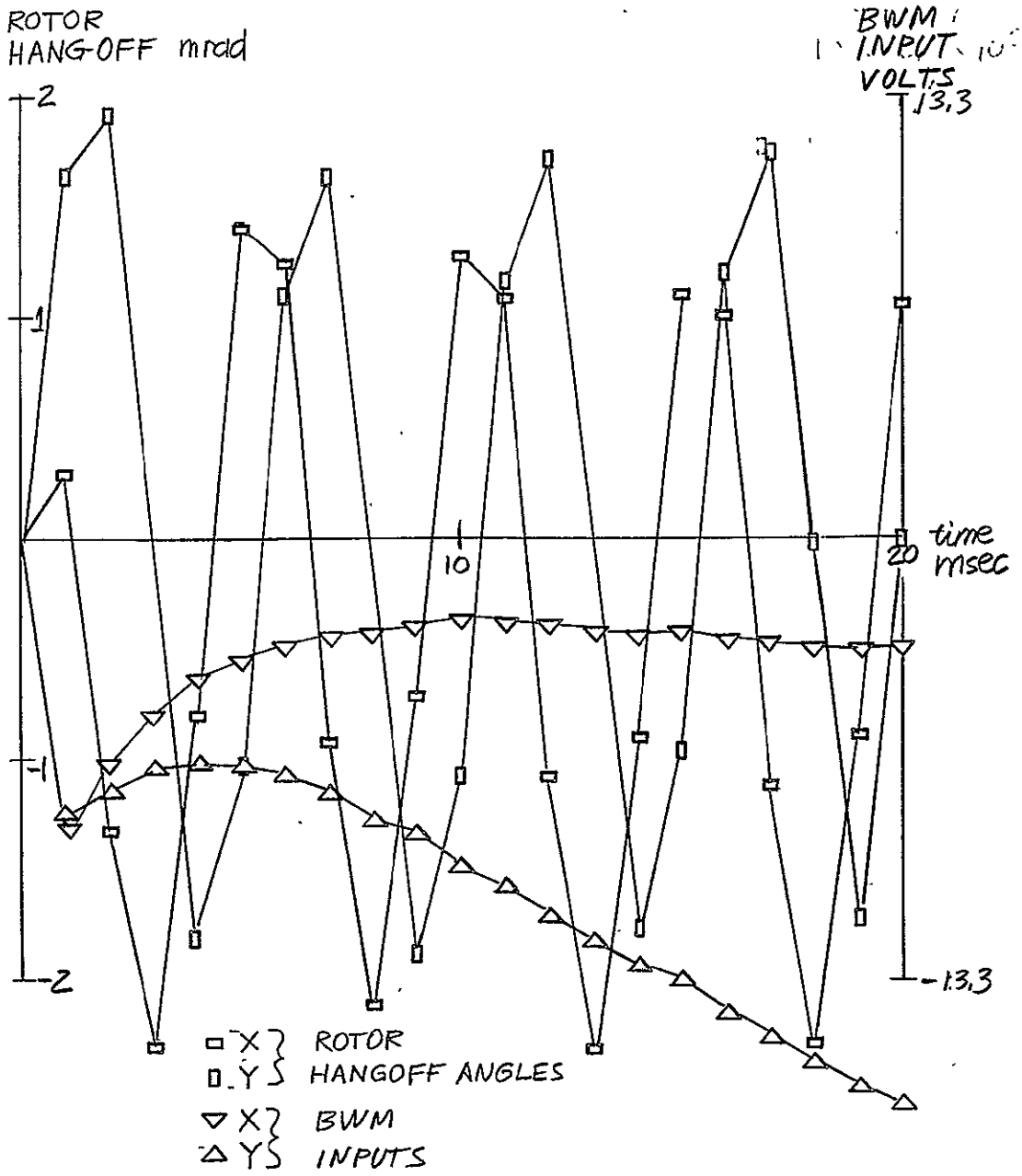

Figure 3-10. Simulation for Digital Noninteracting Loop, Rate

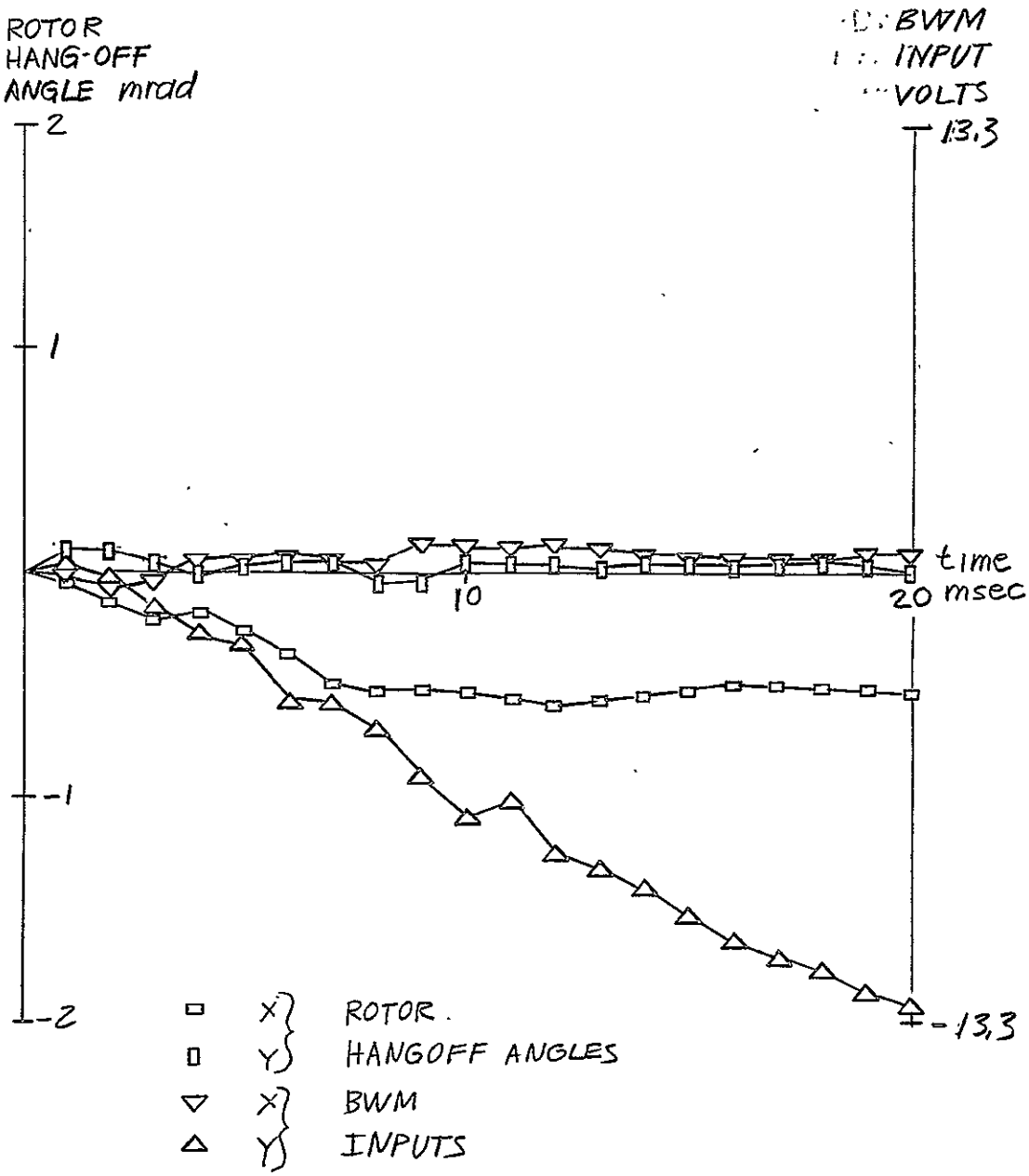

Figure 3-11. Simulation for Digital Teledyne Loop, Rate

Input to X-Axis = 50t, BWM Period = 0.1 msec

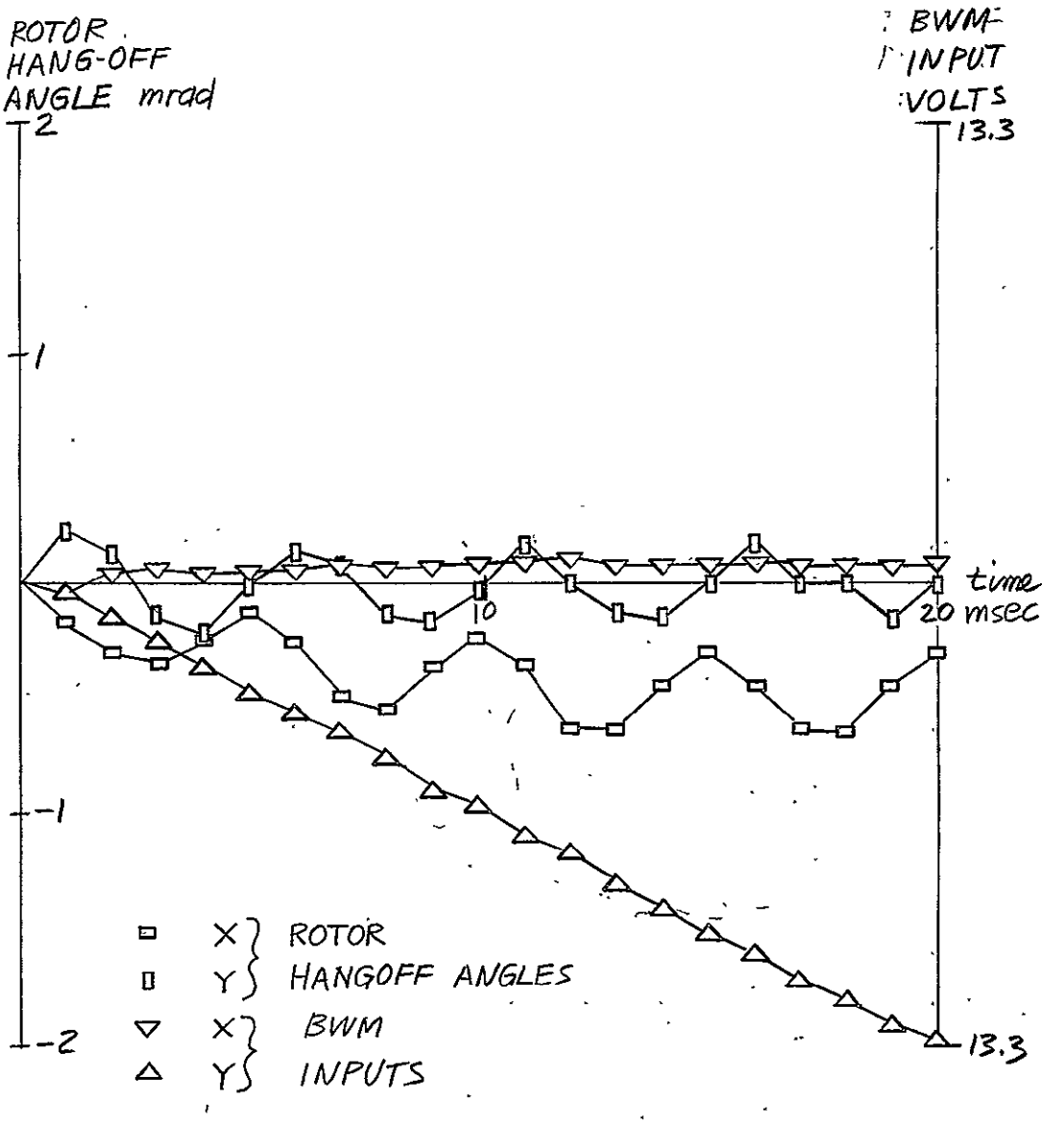

Figure 3-12. Simulation for Digital Noninteracting Loop,

Rate Input to X-Axis = 50t, BWM Period = 0.1 msec

the non-linear element in the loop, in this case the PWM. DF theory is well documented in the literature[11] for single non-linearities within a system, and involves an approximation which linearizes the non-linearity. Ordinarily, a single frequency input to the non-linearity produces an output including this frequency and its harmonics. Most servo loops are considered to be good low pass filters, and the higher harmonics are assumed to be attenuate by the loop. Consequently, only the fundamental frequency of the output of the non-linearity is considered, and its DF may be defined as

$$N(A,\phi) = \frac{\text{Fundamental Harmonic of Output}}{\text{Input}} \quad . \tag{3-4}$$

The system of Figure 3-13 is separated into its linear $L(\omega)$, and non-linear, $N(A,\phi)$, components where A is input amplitude to the non-linearity, ω the frequency, and ϕ the phase angle of N, and if the input to the system is zero,

$$1 + L(\omega)\, N(A,\phi) = 0. \tag{3-5}$$

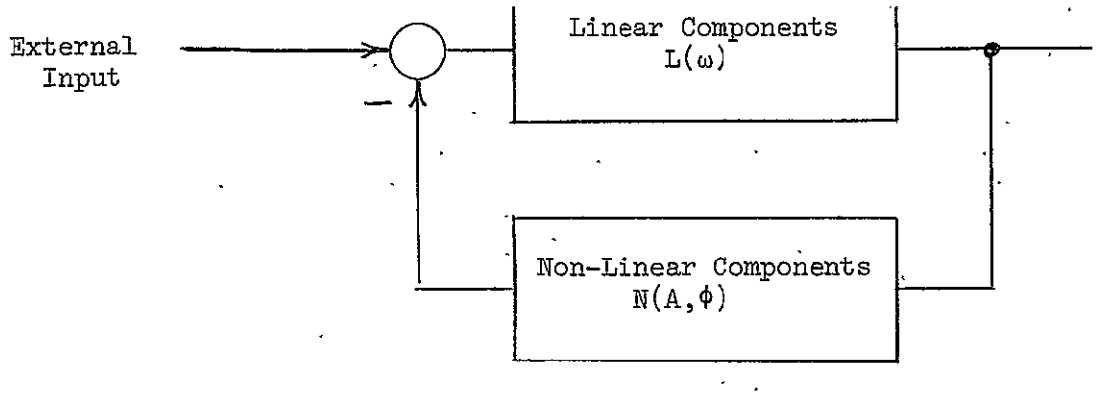

Figure 3-13. Equivalent Loop With Non-Linearity

Equation (3-5) is generally solved graphically by plotting the linear portion $L(\omega)$ on an amplitude-phase plot of $-1/N(A,\phi)$. Permissible limit cycles occur at the intersection of the $L(\omega)$ and $-1/N(A,\phi)$ curves.

In a sampled system, further constraints are placed on the permissible limit cycles. The period of the limit cycle must be some integral multiple of the sampling period, and in the case of a loop which contains at least one integration, this multiple must be even.

For a sampled system using a BWM as its non-linearity, Figure 3-14 shows the lower bounds of limit cycles with periods of 2 through 8 times the sampling period. If the operating point of the linear portion, $L(\omega)$, lies above one of these boundaries, then that limit cycle can exist.

For systems with multiple non-linearities, DF theory generally cannot be used, unless some unusual property is present. Fortunately, the noninteracting design effectively decouples one BWM from the other, so that DF theory may be used on the single-input-single-output equivalent loop. Figure 3-15 shows a plot of (3-3) on Figure 3-14. Because (3-3) represents a type II system, its phase approaches $-180°$ for low frequencies, making low frequency limit cycles unavoidable. For this reason a type I system is desirable, and modification of the feedback loop to make the system type I includes a lag network with a pole at $s = -14$ and zero at $s = -200$, so that the closed loop bandwidth can remain unchanged. The transfer function for this type I system is

$$\frac{\theta_x(s)}{\dot{\phi}_x(s)} = \frac{8000(s/200 + 1)}{s(s/14 + 1)(s/10000 + 1)} \qquad (3\text{-}6)$$

and is also plotted in Figure 3-15. At low frequencies, the phase of this type I system approaches $-90°$, and low frequency limit cycles can be avoided. For a digital rebalance loop employing BWM, the linear portion of the loop must be type I.

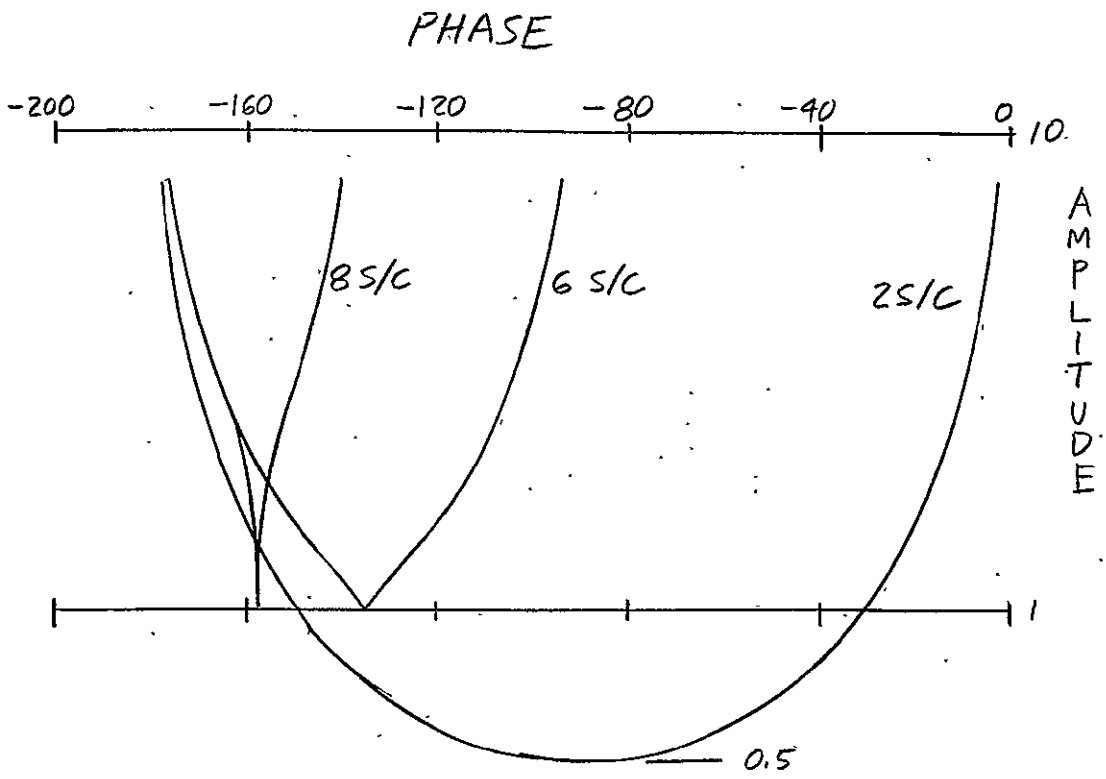

Figure 3-14. Boundary of $-1/N(A,\phi)$ for BWM for Various Limit Cycle Modes

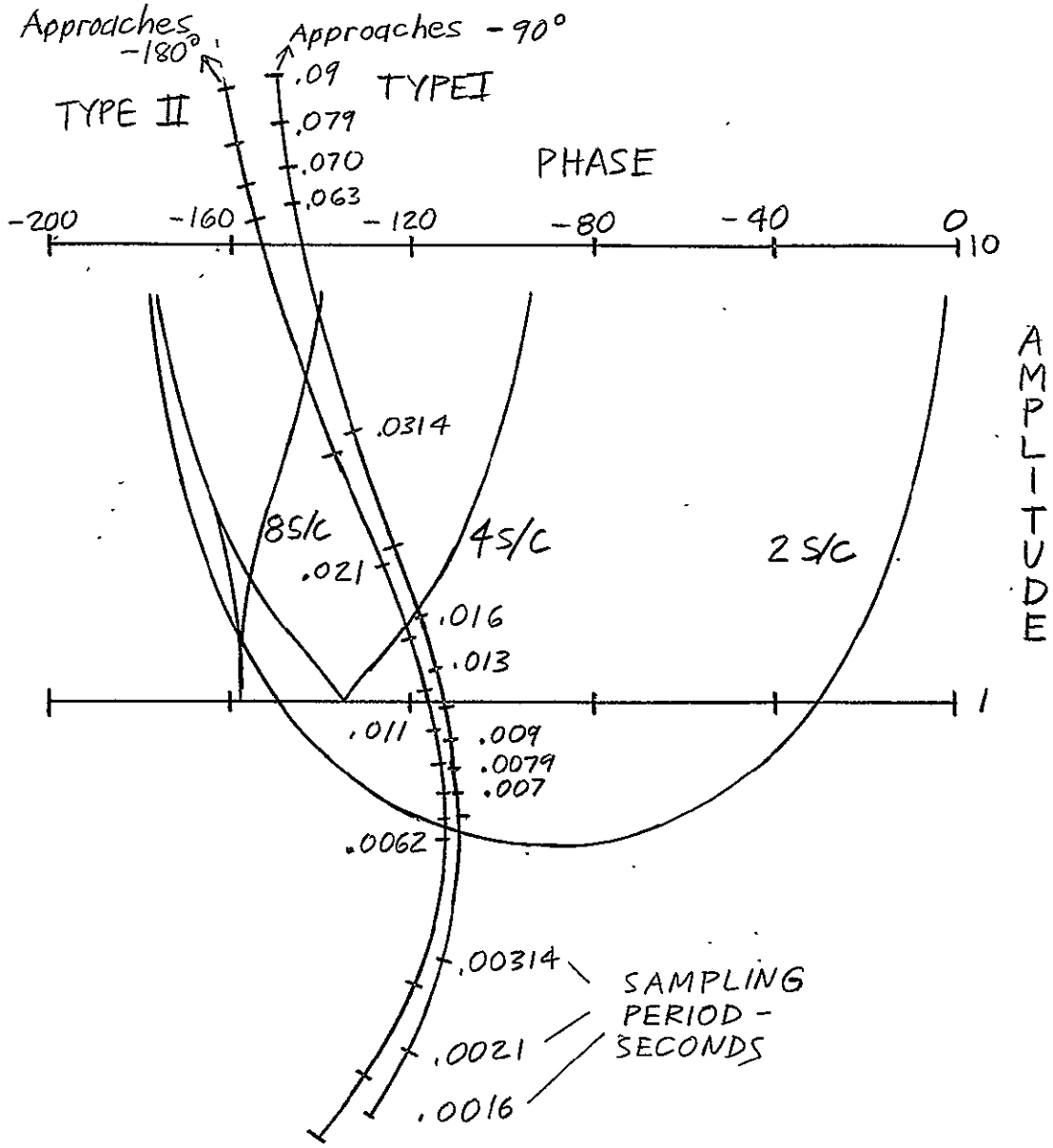

Figure 3-15. Amplitude - Phase Plots of Typical Type I and II Linear Systems Plotted on Boundaries of $-1/N(A,\phi)$

Comparison of Types I and II Loops

In practice, the requirement of zero steady-state rotor hangoff error to constant angular velocity input is unnecessary, a small constant error can be tolerated. Although angular acceleration inputs are experienced in practice, their time integral is sufficiently small that the rotor will not hit its stops in a properly designed loop.

Regardless of whether the response of the rotor hangoff angle to case motion is type I or II, the response at the input to the torquers is the same for a given motion input. The principle of conservation of momentum causes the gyro to process with an angular velocity, $\underline{\omega}$, when torque, $\underline{T}$, is applied, according to the relation

$$\underline{T} = \underline{\omega} \times \underline{H} \qquad (3\text{-}7)$$

where $\underline{H}$, the rotor momentum, is the product of the spin velocity and spin-axis moment of inertia. For a constant velocity input to the x-axis, a constant restoring torque from the y-axis torquer is necessary to rebalance the gyro, independent of whether steady-state rotor hangoff angles are allowed for this input.

CHAPTER IV

PROPOSED PTSA LOOP FOR THE DRY TUNED TDF GYRO AND CONCLUDING REMARKS

I. DIGITAL REBALANCE IMPLEMENTED FOR THE TELEDYNE GYRO

The digital rebalance loop of Figure 4-1 gives the single-input-single-output transfer function,

$$\frac{\theta_x(s)}{\dot{\phi}_x(s)} = \frac{8000(s/200 + 1)}{s(s/14 + 1)(s/10000 + 1)(s/20000 + 1)} \quad , \qquad (4\text{-}1)$$

which is similar to (3-6) except for the pole at s = -20000. This response is type I, but the pole at s = -14 gives the same mid-frequency response as the type II system described by 3-3.

The Teledyne gyro has the physical characteristics shown in Table 4-1.

Symbol	Description	Value
K_T	Torquer Scale Factor	20.1°/amp.sec
K_p	Pickoff Scale Factor	2.26 volts/°
A	Cross-axis Moment of Inertia	800 gm cm^2
C	Spin-axis Moment of Inertia	1500 gm cm^2
N	Spin Frequency	100 Hz (638 rad/sec)
H	Angular Momentum	10^6 gm cm^2/sec
R_T	Torquer Coil Resistance	12 ohm

Table 4-1: Teledyne Gyro Characteristics.

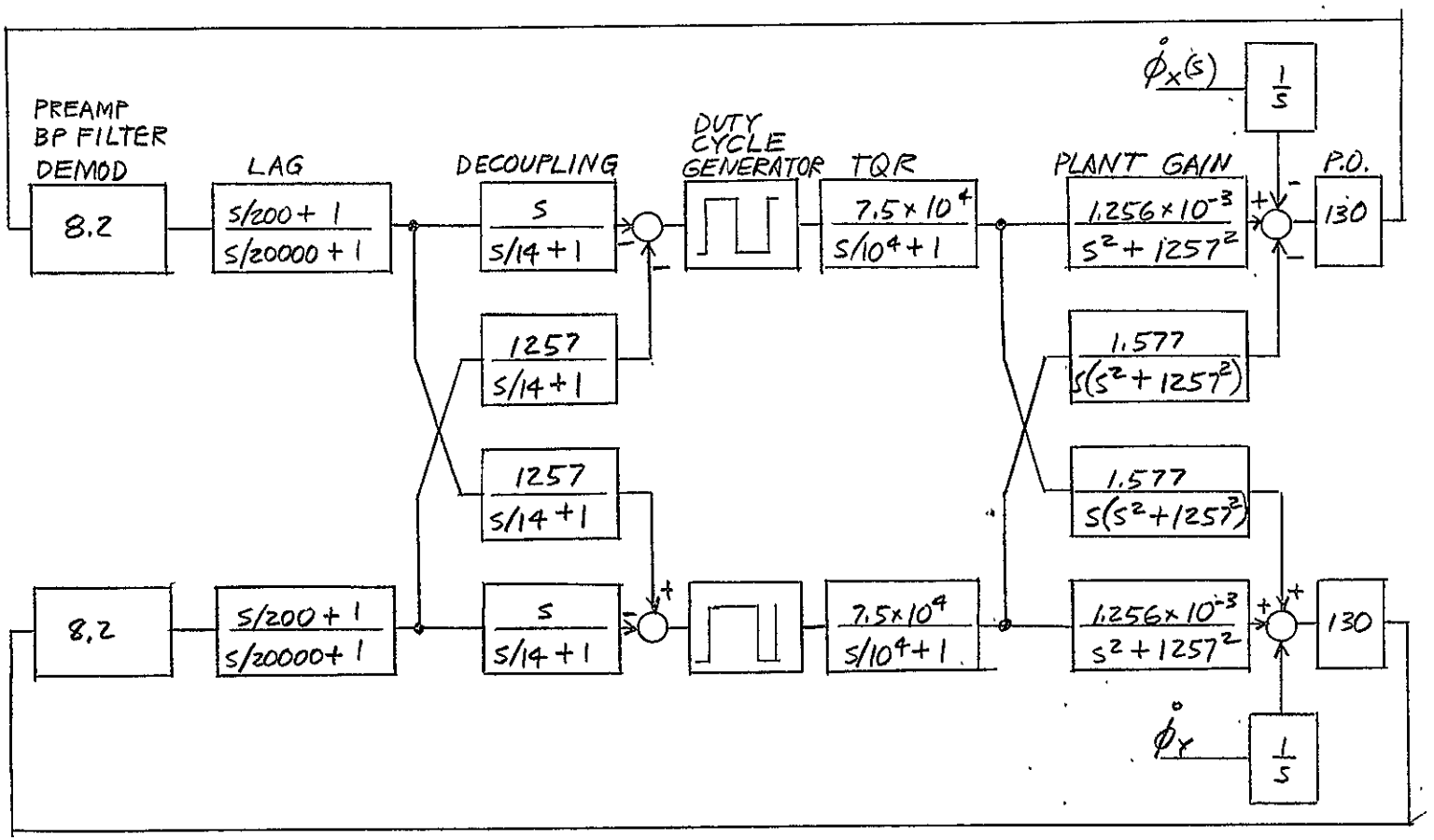

Figure 4-1. Digital Rebalance Loop Using UT Electronics

These characteristics constrain the digital rebalance loop, which is the U.T. modification of the Hamilton Standard design.[12] This loop, a BWM design originally developed for floated, gas spin bearing, SDF gyros, has been adapted to accelerometers as well.

From the physical characteristics of the gyro, the non-interacting design transfer function of (4-1) and the design procedures outlined in Reference 12 for the U.T. loop, the following considerations must be observed:

1. Two channels of the equivalent rebalance loop for an SDF gyro are needed, as well as additional components for decoupling.

2. The rather large rotor angular momentum of 10^6 gm cm^2/sec requires a large rebalance torque. A rate input of 60°/sec requires 3 amperes of torquing current and over 100 watts of power to the torquer coil.

3. The ramp slope constraint simply assumes that the error signal at the input to the BWM does not change faster than the ramp with which it is compared. Thus the ramp

$$R > K_{pc} K_t K_p I, \qquad \text{(13 of Ref. 12)}$$

where K_{pc} does not include the gain A in the decoupler.

4. The interrogation or sampling period, t_i, of the BWM puts a more stringent requirement on the closed loop bandwidth via the ramp slope constraint than through the Nyquist sampling frequency. This relation is

$$f_{cl}\Big|_{max} = \frac{f_i}{\pi} \qquad \text{(16 of Ref. 12)}$$

where f_i is $1/t_i$.

5. The gain, K_{pc}, is found from (8) of Ref. 12 at $\omega = 1$.

$$G(\omega = 1) = \frac{2 K_t K_{pc} K_p I}{R t_i} \qquad (4\text{-}2)$$

where I is the torquer current in amperes, and $G(\omega = 1)$ is 8000. K_{pc} does not include the gain A.

Figure 4-2 shows a block diagram which uses the U.T. rebalance loop with a few additional components. The gain of 24000 is the produc of A = 800 and K_{pc} = 30 from (4-2). The interrogation period, t_i, is 0.1 msec to avoid limit cycles and provide sufficient closed loop bandwidth.

The data resolution of the loop can be stated as

$$\Delta\theta_d = 7200 \frac{\text{Maximum Rebalance Rate}}{\text{Data Rate}} \text{ (arc sec)} \qquad (4\text{-}3)$$

and is 0.7 arc sec for a 60°/sec maximum rebalance rate and 614.4 kHz data rate. This resolution may be improved by dual mode operation of the torquer current, or by increasing the data rate.

II. CONCLUSIONS

This report includes the investigation of the feasibility of using a PTSA rebalance loop for a dry, tuned TDF gyro in the strapdown mode. This strapdown TDF gyro would be a welcome addition to the famil of sensors available for spacecraft navigation.

Also included is a derivation for transfer function of this gyro including the conditions of tuning for both the single and two gimbal cases. The single gimbal gyro is not a true "tuned" gyro, since its tuning condition contains rotor inertia terms, except in the special (and physically unrealizable) case where the rotor is infinitesimally thin, causing the C-2A term involving rotor inertias to vanish from the tuning equation. In the strict sense, tuning is a function of speed, gimbal inertias, and the torsional spring constants of the restraints, and this can occur for a physically realizable rotor only when the gyro has more than one gimbal.

Two analog rebalance loops for this gyro were simulated. These loops were converted to the digital mode by the addition of binary width modulators to digitize the torquer currents. Although these loops performed well at the higher sampling rate of 10 kHz, the

recommended final design for a digital rebalance loop for this gyro should be Type I, to assure operation without low frequency limit cycles.

A conceptual type I design using a modified version of the U.T. rebalance electronics is given in the preceeding section of this chapter. While this design is feasible, the gyro used in the loop has poor characteristics for a high rate environment, requiring excessive power to the torquer coils. However, the concept of digital rebalance for a dry tuned TDF gyro is sound, and awaits a gyro with suitable characteristics.

LIST OF REFERENCES

1. Edwards, A., "The State of Strapdown Inertial Guidance and Navigation," Navigation Journal of the I.O.N., Winter 1971-1972, vol. 18 #4, pp 386-401.

2. Howe, E.W., "A Free Rotor Gyro," Symposium on Unconventional Inertial Sensors, Farmingdale, N.Y., 1963.

3. Howe, E.W., and Savet, P.H., "The Dynamically Tuned Free Rotor Gyro," Control Engineering, June 1964, pp 67-72.

4. Savet, P.H., "Dynamics of Ideal Suspensions Applied to Rotating Bodies in Space," AIAA 2nd Annual Meeting, Paper #65-435, July 1965.

5. Cimera, R.F. and Napolitano, M., "The Gyroflex Gyroscope--An Unconventional Sensor" Symposium on Unconventional Inertial Sensors, Farmingdale, N.Y., 1969.

6. Lipman, J.S., "Application of the Complex Method to Transform Analysis of Spinning Systems with Rotating Nonsymmetries," Joint Automatic Control Conference of the American Automatic Control Council, June 1968, pp 102-108.

7. Craig, R.J.G., "Theory of Operation of An Elastically Supported, Tuned Gyroscope," IEEE Transactions on Aerospace and Electronic Systems, vol. AES-8, No. 3, May 1972, pp 280-288.

8. Craig, R.J.G., "Dynamically Tuned Gyros in Strapdown Systems," N.A.T.O. - A.G.A.R.D. Conference Proceedings No. 116 on Inertial Navigation Components and Systems, February 1973.

9. Chen, K., Mathias, R.A., Sauter, D.M., "Design of Noninteracting Control Systems Using Bode Diagrams," A.I.E.E. Trans., Pt. II, January 1962, pp 336-346.

10. Hung, J.C., and Rowe, W.L., Scientific Report S-23, "A Study of Strapdown Platform Technology," Chapter 2, NASA Contract No. NAS8-27296/DCN 1-1-40-10230, Department of Electrical Engineering, The University of Tennessee, Knoxville, Tennessee, April 15, 1972.

11. Gelb, A., and Vander Velde, W.E., "Multiple-Input Describing Functions and Nonlinear System Design," McGraw-Hill Book Co., New York, 1968.

12. Blalock, T.V., Kennedy, E.J., and McKnight, R.D., Scientific Report S-25, "Development of a Width-Modulated Pulse Rebalance Electronics Loop for Strapdown Gyroscopes," NASA Contract No. NAS8-27296/DCN 1-1-40-10230, Department of Electrical Engineering, The University of Tennessee, Knoxville, Tennessee, July 13, 1973.

APPENDIX I

A USEFUL COMPLEX CONJUGATE PROPERTY

If $B(s) = A(s - j\gamma)$, then $\overline{B}(s) = \overline{A}(s + j\gamma)$.

Proof:

Let j be the imaginary rotation for the spatial domain, and i be the imaginary rotation for the time domain. The Laplace transform variable $s = \gamma + i\beta$.

$$a(t) \triangleq x(t) + jy(t), \quad A(s) = X(s) + jY(s)$$

therefore

$$\overline{a}(t) = x(t) - jy(t), \text{ and } \overline{A}(s) = X(s) - jY(s).$$

Let

$$b(t) \triangleq a(t)\varepsilon^{j\gamma t} = (x(t) + jy(t))\cdot\varepsilon^{j\gamma t}$$

then

$$\overline{b}(t) = \overline{a}(t)\varepsilon^{-j\gamma t} = (x(t) - jy(t))\cdot\varepsilon^{-j\gamma t}$$

and

$$B(s) = X(s - j\gamma) + jY(s - j\gamma) = A(s - j\gamma),$$

$$\overline{B}(s) = X(s + j\gamma) - jY(s + j\gamma) = \overline{A}(s + j\gamma).$$

Q.E.D.